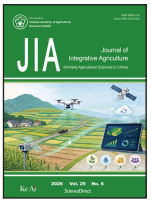
Journal of Integrative Agriculture 2026, 25(6): 2580–2594

KeAi CHINESE ROOTS GLOBAL IMPACT

Available online at ScienceDirect

Journal of Integrative Agriculture



RESEARCH ARTICLE

Parallel denitrification and nitrite oxidation in the unsaturated zone: Isotopic constraints from nitrate $\delta^{15}N$ and $\delta^{18}O$ in Tianjin, China

Dongmei Xue[1*], Jinglei Wang[1*], Lanxin Xiang[1], Xiaoxian Peng[1], Ke Jin[2#], Yunting Fang[3#], Xiangzhen Li[4], Yidong Wang[1], Zhongliang Wang[5]

[1] *Tianjin Key Laboratory of Water Resources and Environment, Tianjin Normal University, Tianjin 300387, China*
[2] *Institute of Grassland Research, Chinese Academy of Agricultural Sciences, Huhhot 010010, China*
[3] *Key Laboratory of Forest Ecology and Management, Institute of Applied Ecology, Chinese Academy of Sciences, Shenyang 110016, China*
[4] *College of Resources and Environment, Fujian Agriculture and Forestry University, Fuzhou 350002, China*
[5] *Tianjin Key Laboratory of Aquatic Science and Technology, Tianjin Chengjian University, Tianjin 300384, China*

Highlights

- Nitrate reduction drives isotope trajectory variation.
- Carbon properties regulate N functional gene expression.
- The $\Delta\delta^{18}O$:$\Delta\delta^{15}N$ trajectory is effective for assessing denitrification performance.

Abstract

Denitrification plays a critical role in mitigating anthropogenic nitrate (NO_3^-) accumulation in ecosystems. The isotopic composition of NO_3^- ($\delta^{15}N$ and $\delta^{18}O$) serves as a powerful tracer for identifying N sources and transformation processes. Denitrification often superimposed on the isotope effects of NO_2^- oxidation, resulting in parallel enrichment of $\delta^{15}N$- and $\delta^{18}O$-NO_3^- ($\Delta\delta^{18}O$:$\Delta\delta^{15}N$ trajectory) that causes them to be either below or above 1. This study compared the $\Delta\delta^{18}O$:$\Delta\delta^{15}N$ trajectory during denitrification, functional genes (*narG*, *napA*, and *nxrA*), and carbon sources from metabolites in the $\Delta\delta^{18}O$:$\Delta\delta^{15}N$ trajectories below or above 1 in unsaturated zones. The results revealed that NO_3^- reduction was more important for variation in the $\Delta\delta^{18}O$:$\Delta\delta^{15}N$ trajectory because the difference in isotope effects ($^{15}\varepsilon_{NO_3\ reduction}$ and $^{18}\varepsilon_{NO_3\ reduction}$) between the two $\Delta\delta^{18}O$:$\Delta\delta^{15}N$ trajectory groups was significant, whereas the difference in isotope effects ($^{15}\varepsilon_{nxr}$ and $^{18}\varepsilon_{nxr}$) upon NO_2^- oxidation was not. Carbon sources in the group with $\Delta\delta^{18}O$:$\Delta\delta^{15}N$ trajectories below 1 facilitated more efficient electron production to promote NO_3^- reduction because of their low molecular weight and simple structure. Conversely, the lower electron production efficiency due to the high molecular weight and complex structures of carbon sources in the group with $\Delta\delta^{18}O$:$\Delta\delta^{15}N$ trajectories above 1 downregulated the expression of the three functional genes (*narG*, *napA*, and *nxrA*). The group with $\Delta\delta^{18}O$:$\Delta\delta^{15}N$ trajectories below 1 showed significantly higher levels of $^{15}\varepsilon_{NO_3\ reduction}$, $^{18}\varepsilon_{NO_3\ reduction}$, NO_2^- oxidation ratio, and copy numbers of *narG*, *napA*, and *nxrA* genes compared to the other group, revealing that NO_3^- reduction at the cellular level was more active in the former group. This study elucidated the integrated influence of isotope effects, NO_3^- reductase and NO_2^- oxidoreductase activities, and carbon sources from metabolites. These findings are significant for understanding the $\Delta\delta^{18}O$:$\Delta\delta^{15}N$ trajectories of N cycling in terrestrial ecosystems and support groundwater conservation by improving carbon supplementation approaches that stimulate denitrification, with $\Delta\delta^{18}O$:$\Delta\delta^{15}N$ trajectories serving as effective tracers for assessing denitrification performance in terrestrial environments.

Keywords: denitrification, NO_2^- oxidation, $\Delta\delta^{18}O$:$\Delta\delta^{15}N$ trajectory, NO_3^- reductase, NO_2^- oxidoreductase, carbon sources

Received 5 May 2025; Received in revised form 13 August 2025; Accepted 27 October 2025; Available online 13 January 2026
Dongmei Xue, E-mail: xuedongmei@tjnu.edu.cn; Jinglei Wang, E-mail: 17861007620@163.com; #Correspondence Ke Jin, E-mail: jinke@caas.cn; Yunting Fang, E-mail: fangyt@iae.ac.cn
* These authors contributed equally to this study.

© 2026 CAAS. Publishing services by Elsevier B.V. on behalf of KeAi Communications Co. Ltd. This is an open access article under the CC BY-NC-ND license (http://creativecommons.org/licenses/by-nc-nd/4.0/). Peer review under responsibility of Editorial Board of *Journal of Integrative Agriculture*.
doi: 10.1016/j.jia.2026.01.010

1. Introduction

The widespread accumulation of nitrate (NO_3^-) from anthropogenic nitrogen (N) inputs has threatened ecosystems through eutrophication, acidification, and groundwater contamination (Gruber and Galloway 2008; Xue *et al.* 2009; Zheng *et al.* 2020; Singh *et al.* 2022). Consequently, comprehensive understanding of denitrification (the microbially-mediated reduction of NO_3^- to N_2) becomes fundamentally important for ecosystem management strategies.

Stable isotopes ($\delta^{15}N$ and $\delta^{18}O$) of NO_3^- provide key insights into denitrification mechanisms, as this process preferentially removes lighter isotopes (^{14}N and ^{16}O), enriching residual NO_3^- in ^{15}N and ^{18}O along a predictable trajectory ($\Delta\delta^{18}O$:$\Delta\delta^{15}N$). This coupled isotopic signature serves as a unique fingerprint of denitrification, unaffected by variations in pH, salinity, or organic carbon availability (Granger *et al.* 2008; Kritee *et al.* 2012; Wunderlich *et al.* 2013).

When expressed as $\Delta\delta^{18}O$:$\Delta\delta^{15}N$, the classical fractionation range of $\Delta\delta^{15}N$:$\Delta\delta^{18}O$ (1.3–2.1) corresponds to values between 0.48 and 0.77 (Böttcher *et al.* 1990). Notably, a canonical value of $\Delta\delta^{18}O$:$\Delta\delta^{15}N$ below 1 is widely used for denitrification occurring in pure batch cultures, freshwater, groundwater, and soil systems (Wenk *et al.* 2014; Fang *et al.* 2015; Paredes *et al.* 2020; Valiente *et al.* 2020; Bao *et al.* 2024), whereas a $\Delta\delta^{18}O$:$\Delta\delta^{15}N$ value close or equal to 1 is used in marine environments (Sigman *et al.* 2006; Karsh *et al.* 2012; Harms *et al.* 2019). The striking difference in this ratio has been attributed to fractionation during enzymatic bond breakage by three NO_3^- reductases: bacterial membrane-bound dissimilatory (Nar), cytosolic assimilatory (Nas), and periplasmic dissimilatory (Nap) reductases (Treibergs and Granger 2017; Asamoto *et al.* 2021). NO_3^- reduction catalyzed by Nar and Nas fractionates N and O isotopes in a nearly equal manner (Granger *et al.* 2008, 2010; Karsh *et al.* 2012). The activity of membrane-bound Nar is apparently high during anaerobic growth, identifying Nar as a likely driver of isotope enrichment during NO_3^- reduction to NO_2^- both in terrestrial and marine environments (Pinchbeck *et al.* 2019; Pandey *et al.* 2020; Zhang *et al.* 2022); whereas, Nas is not considered the dominant enzyme in research analyses. However, NO_3^- reduction mediated by Nap also proceeds with a $\Delta\delta^{18}O$:$\Delta\delta^{15}N$ trajectory below 1 (Frey *et al.* 2014), with reported values of 0.6 according to Granger *et al.* (2008) and 0.5 according to Wenk *et al.* (2014) and can be found mainly in terrestrial ecosystem.

In recent years, $\Delta\delta^{18}O$:$\Delta\delta^{15}N$ trajectories above 1 have been found in marine environments as well (Buchwald *et al.* 2015; Casciotti 2016; Kemeny *et al.* 2016; Sun *et al.* 2017), associated with NO_2^- oxidation during NO_3^- reduction to NO_2^- in denitrification. Although NO_2^- oxidizers are obligately aerobic, NO_2^- can also be oxidized to NO_3^- in anaerobic or anoxic environments (Lipschultz *et al.* 1990; Füssel *et al.* 2012). As the key enzyme in nitrite-oxidizing bacteria (NOB), nitrite oxidoreductase (Nxr) is an integral membrane protein that exists in both cytoplasmic and periplasmic forms. This enzyme facilitates the coupled intracellular oxidation of NO_2^- and reduction of NO_3^- (Wunderlich *et al.* 2013; Kemeny *et al.* 2016; Chicano *et al.* 2021; Lycus *et al.* 2023). In NO_2^- oxidation, an inverse kinetic isotope effect occurs as the heavier isotopes ^{15}N and ^{18}O are preferentially enriched in the newly generated NO_3^- (Casciotti 2009, 2013; Buchwald and Casciotti 2010; Kobayashi *et al.* 2019). Granger and Wankel (2016) presented a multi-process numerical model of dual NO_3^- isotope dynamics to improve the overall understanding of $\Delta\delta^{18}O$:$\Delta\delta^{15}N$ deviation from the expected 1:1 trajectory of denitrification in different ecosystems. It was hypothesized that $\Delta\delta^{18}O$:$\Delta\delta^{15}N$ trajectories above 1 should primarily occur in the marine because the ^{18}O values of seawater are significantly higher than the ^{18}O values of water in terrestrial ecosystems (Casciotti 2009; Buchwald and Casciotti 2013; Granger and Wankel 2016). This may enhance the enrichment of the heavier ^{18}O isotope in newly generated NO_3^- during NO_2^- oxidation, resulting in $\Delta\delta^{18}O$:$\Delta\delta^{15}N$ trajectories above 1. Conversely, terrestrial ecosystems are expected to have $\Delta\delta^{18}O$:$\Delta\delta^{15}N$ trajectories below 1 (Frey *et al.* 2014; Asamoto *et al.* 2021).

However, NO_3^- reduction and NO_2^- oxidation are mainly driven by functional genes (*narG*, *napA*, and *nxrA*) encoding NO_3^- reductase, as well as by NO_2^- oxidoreductase and microbial communities possessing these genes that widely occur in terrestrial systems (González *et al.* 2006; Daims *et al.* 2015). Microorganisms survive and proliferate using various metabolic pathways; metabolites in the environment can be involved in microbial activities as carbon sources to provide electrons and energy for denitrification (Moran *et al.* 2022). This provision of carbon sources may up- or downregulate the expression of corresponding functional genes (Fig. 1) and act on N and O isotopic fractionation as the bonds of NO_3^- break and form during enzymatic activity. Therefore, we hypothesized that the $\Delta\delta^{18}O$:$\Delta\delta^{15}N$ trajectory in terrestrial ecosystems would vary over a broader range below and above 1. Moreover, NO_3^- reduction and NO_2^- oxidation processes might differ in the two $\Delta\delta^{18}O$:$\Delta\delta^{15}N$ trajectory types.

To better understand these dynamics, we selected the unsaturated zone as a vital component of soil ecosystem. An integrated approach was used to combine a multi-process numerical model of dual NO_3^- isotope dynamics, functional genes, and metabolomics analyses to investigate the difference in isotope effects, ratios of NO_2^- oxidation during NO_3^- reduction, functional genes (*narG*, *napA*, and *nxrA*), and carbon sources in $\Delta\delta^{18}O$:$\Delta\delta^{15}N$ trajectories below and above 1. This study is expected to enhance the overall understanding of how NO_3^- attenuation processes influence the N cycle $\Delta\delta^{18}O$:$\Delta\delta^{15}N$ trajectory in terrestrial ecosystems. It also offers key insights for groundwater conservation by optimizing carbon amendment approaches, which stimulate microbial NO_3^- removal while allowing denitrification efficiency to be tracked by $\Delta\delta^{18}O$:$\Delta\delta^{15}N$ trajectories as indicators.

2. Materials and methods

2.1. Study area

The study sites were located in the coastal municipality of Tianjin, China. The present shape of this municipality was formed by several historical seawater intrusions and

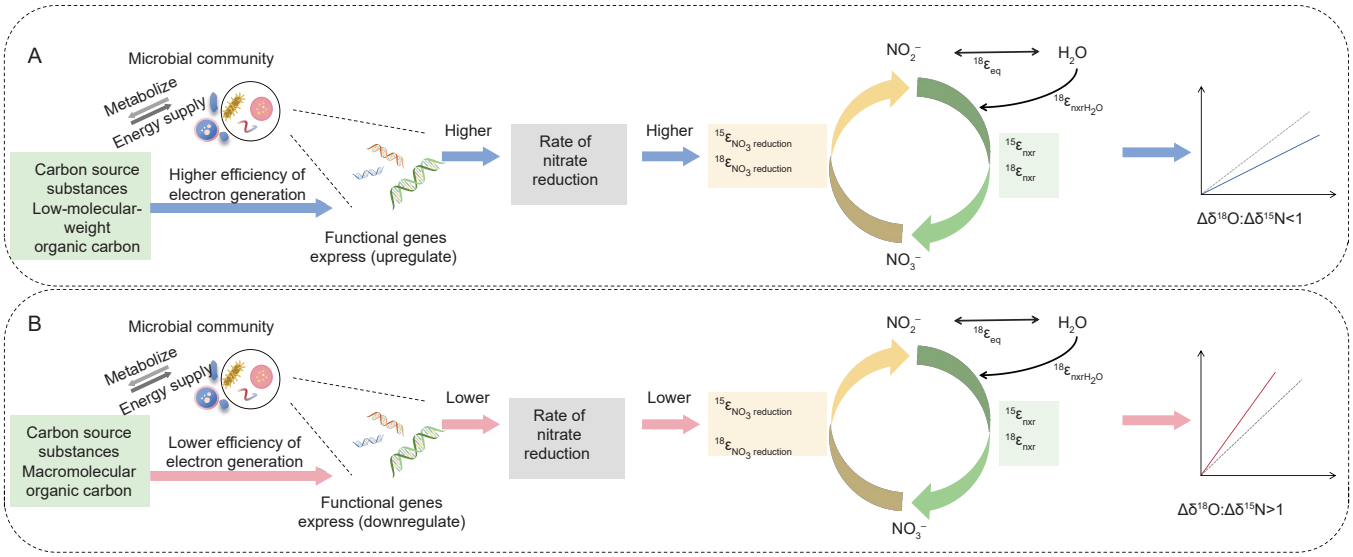


Fig. 1 Effects of low-molecular-weight (A) and macromolecular (B) carbon sources on the variation in $\Delta\delta^{18}O:\Delta\delta^{15}N$ trajectories. $^{15}\varepsilon_{NO_3\ reduction}$, N isotope effect on NO_3^- reduction by denitrifiers; $^{18}\varepsilon_{NO_3\ reduction}$, O isotope effect on NO_3^- reduction by denitrifiers; $^{15}\varepsilon_{nxr}$, N isotope effect on NO_2^- oxidation by nitrifiers; $^{18}\varepsilon_{nxr}$, O isotope effect on NO_2^- oxidation by nitrifiers; $^{18}\varepsilon_{nxrH_2O}$, O isotope effect for H_2O incorporation by nitrifiers; $^{18}\varepsilon_{eq}$, equilibrium isotope effect between NO_2^- and H_2O.

regressions (Wang *et al.* 2000, 2007). Parts of the central and southern areas were below sea level 4,000–5,000 years ago, and the soil in this area was greatly affected by seawater. The study area has a warm-temperate semi-humid continental monsoon climate with annual precipitation of 520–660 mm (75% of the total precipitation occurs from June to August) and an annual average temperature of 11.4–12.9°C (Yue *et al.* 2010).

The N cycle and associated biogeochemical characteristics in the study area have been extensively investigated across multiple dimensions, encompassing but not limited to: (1) Microbial-mediated processes. Soil N dynamics are dominated by NO_3^- reduction (denitrification) and production (nitrification), with denitrification exhibiting particularly high activity in the unsaturated zone (0–3 m depth) under neutral pH conditions (Wang *et al.* 2017; Xue *et al.* 2020). Coastal wetland conversion (e.g., tidal flats and *Spartina alterniflora* marshes transformed into aquaculture ponds) significantly reduces comammox bacterial diversity and alters community structure (Tan *et al.* 2023). (2) Agricultural impacts. Long-term fertilizer application has induced N accumulation in farmland soils, elevating risks of N leaching and greenhouse gas emissions (Hu *et al.* 2022; Zhao *et al.* 2024). (3) Pollution and salinization effects. Heavy metal contamination inhibits microbial activity, thereby reducing organic matter decomposition rates and indirectly impairing N transformation efficiency (Liu *et al.* 2017; Zhu *et al.* 2023). In saline-alkali soils, salt stress decreases N utilization efficiency and is associated with reduced soil organic carbon contents (Zhu *et al.* 2020). Based on literature integration and previous research findings from the research group, with a focus on multi-factor coupling mechanisms, five sampling points were selected in the unsaturated zone: three sites in braunerde and fluvo-aquic soil areas not influenced by seawater and two sites in coastal saline soil areas influenced by historical seawater intrusion and regression.

2.2. Sampling and analyses

The sampling campaign was conducted in May 2023. Unsaturated zone cores were collected with a 5.5-cm-diameter hollow-stem hand auger. Samples were collected from the ground surface to a depth of 3 m at 0.3-m intervals (the groundwater table was located at a depth of 4.0 m). At each sampling location, five drill cores collected at 5-m intervals were homogenized to form one composite soil sample. Samples were hermetically sealed in polyethylene bags and transported to the laboratory on ice. Soil pH and salinity were determined in a 1:2.5 mixture of soil and deionized water with a portable probe (Orion Star A329, Thermo, USA). Soil organic carbon (SOC) and total nitrogen (TN) were determined with a total organic carbon analyzer (Vario, Elementar, Germany). Ammonium (NH_4^+), nitrite (NO_2^-), and NO_3^- were extracted using 2 mol L^{-1} KCl, and the contents were determined with a continuous flow analyzer (Auto Analyzer 3, Seal, Germany). Portions of the soil samples were stored at −80°C for genomic DNA extraction.

In the determination of $\delta^{15}N\text{-}NO_3^-$ and $\delta^{18}O\text{-}NO_3^-$ in NO_3^-, sulfamic acid was employed to remove NO_3^- from the samples, following the method described by Granger and Sigman (2009). At room temperature, a measured mass of sulfamic acid solid was dissolved in ultrapure water, followed by addition of 10% (v/v) hydrochloric acid to prepare a 10 mmol L^{-1} sulfamic acid reagent (pH 1.61.8). Subsequently, 5 mL of sample was combined with 5 mL of the sulfamic acid reagent in a centrifuge tube and allowed to react for 15–20 min. The mixture was then neutralized by adding sodium hydroxide solution (2 mol L^{-1}). Finally, the treated samples were cryopreserved for subsequent isotopic analysis. Subsequently, the N and O isotopic values of NO_3^- were determined *via* bacterial denitrification

(Sigman *et al.* 2001; Casciotti *et al.* 2002; Xue *et al.* 2010), which can simultaneously determine the $\delta^{15}N$ and $\delta^{18}O$ of N_2O produced from the conversion of NO_3^- by denitrifying bacteria that naturally lack N_2O^- reductase activity. A sample of N_2O is placed in a Finnigan MAT Precon device connected to a Finnigan MAT 252 isotope ratio mass spectrometer. This device performs three steps before the N_2O sample is introduced to the mass spectrometer: the sample is sent through a chemical trap in helium carrier to remove water and carbon dioxide, the N_2O is cryogenically focused, and the resulting N_2O peak is chromatographically separated from any remaining carbon dioxide. In the mass spectrometer, measurements at masses of 44, 45, and 46 allow the coupled measurement of the $^{15}N/^{14}N$ and $^{18}O/^{16}O$ ratios of N_2O, after correction for the contribution of ^{17}O to mass 45.

Stable isotopic values (δ_{sample}) are expressed in delta notation (δ) per mil (‰) relative to international standards:

$$\delta_{sample}(‰)=\left(\frac{R_{sample}}{R_{standard}}-\right)\times1000 \quad (1)$$

where R_{sample} and $R_{standard}$ represent the $^{15}N/^{14}N$ or $^{18}O/^{16}O$ ratio of the sample and standard, respectively. The $\delta^{15}N$ and $\delta^{18}O$ values were relative to atmospheric air (AIR) and Vienna standard mean ocean water 2 (VSMOW 2), respectively. The calibration standards used were the nitrates USGS 32, USGS 34, and USGS 35 supplied by the National Institute of Standards and Technology (Gaithersburg, MD, USA).

2.3. Multi-process numerical model of dual NO_3^- isotope dynamics

Under anaerobic or anoxic conditions, NO_3^- reduction and NO_2^- oxidation affect the coupled N and O isotope trajectories. During the reduction of NO_3^- driven by the enzymes Nar and Nap, kinetic isotope effects are responsible for preferential use of the lighter isotopes ^{14}N and ^{16}O, resulting in progressive enrichment of the NO_3^- pool in ^{15}N and ^{18}O (with normal N and O isotope effects), $^{15}\varepsilon_{NO_3\ reduction}$, and $^{18}\varepsilon_{NO_3\ reduction}$. However, NO_2^- oxidation driven by Nxr has been characterized as an "inverse" kinetic isotope effect; $^{15}\varepsilon_{nxr}$ and $^{18}\varepsilon_{nxr}$, with NO_2^- molecules containing the heavy isotopes ^{15}N and ^{18}O, react more quickly (Casciotti 2009). Two other steps during NO_2^- oxidation affect the $\delta^{18}O$ values in newly produced NO_3^-: a new O atom from H_2O is incorporated, in which $H_2{}^{16}O$ is preferentially added to the NO_2^- over $H_2{}^{18}O$ *via* a kinetic isotope effect ($^{18}\varepsilon_{nxrH_2O}$); O atoms are exchanged between NO_2^- and H_2O through an equilibrium isotope effect ($^{18}\varepsilon_{eq}$). Granger and Wankel (2016) proposed a multi-process numerical model of dual NO_3^- isotope dynamics that includes these N and O isotope effects. The $\delta^{15}N$ and $\delta^{18}O$ values of NO_3^- can be calculated as follows (Granger and Wankel 2016):

$$[^{15}N_{NO_3}]_{(t+1)}=[^{15}N_{NO_3}]_{(t)}+[NXR/^{15}\alpha_{nxr}\times{}^{15}F_{NO_2(t)}-NRR/^{15}\alpha_{NO_3reduction}\times{}^{15}F_{NO_3(t)}]\times dt \quad (2)$$

$$[^{18}O_{NO_3}]_{(t+1)}=[^{18}O_{NO_3}]_{(t)}+[NXR\times(2/3\times{}^{18}F_{NO_2(t)}/{}^{18}\alpha_{nxr}+1/3\times{}^{18}F_{H_2O}/{}^{18}\alpha_{nxrH_2O})-NRR/{}^{18}\alpha_{NO_3reduction}\times{}^{18}F_{NO_3(t)}]\times dt \quad (3)$$

where $[^{15}N_{NO_3}]$ and $[^{18}O_{NO_3}]$ are the content-weighted N and O isotopic values for the NO_3^- pool at time points t and t+1, respectively; NXR is the rate of NO_2^- oxidation to NO_3^-; NRR is rate of NO_3^- reduction to NO_2^-, with $^{15}\alpha_{NO_3\ reduction}$ and $^{18}\alpha_{NO_3\ reduction}$ regarded as the N and O isotope fractionation factors for NO_3^- reduction, respectively; $^{15}\alpha_{nxr}$ and $^{18}\alpha_{nxr}$ are the N and O isotope fractionation factors for NO_2^- oxidation, respectively; $^{18}\alpha_{nxrH_2O}$ is the O isotope fractionation factor for H_2O incorporation; $^{15}F_{NO_2}$ and $^{15}F_{NO_3}$ are the ^{15}N fraction in NO_2^- and NO_3^-, respectively; and $^{18}F_{NO_2}$, $^{18}F_{NO_3}$, and $^{18}F_{H_2O}$ are the respective ^{18}O fractions in NO_2^-, NO_3^-, and H_2O.

Using eqs. (2) and (3), it is possible to simulate the ratio of NO_2^- oxidation (R=NXR/NRR) in a closed system; the N and O isotope effects of NO_3^- reduction to NO_2^-, $^{15}\varepsilon_{NO_3\ reduction}$ and $^{18}\varepsilon_{NO_3\ reduction}$; the N and O isotope effects of NO_2^- oxidation to NO_3^-, $^{15}\varepsilon_{nxr}$ and $^{18}\varepsilon_{nxr}$; and the apparent N isotope effect ($^{15}\varepsilon_{app}$), derived from the change in $\delta^{15}N$-NO_3^- relative to the natural logarithm of the NO_3^- fraction remaining. Table 1 lists the parameters and value ranges used in the model. The model output was restricted to satisfying $^{15}\varepsilon>{}^{18}\varepsilon$, ensuring that the simulated $^{15}\varepsilon_{app}$ results were consistent with the measured $^{15}\varepsilon_{app}$ of the samples, and NRR was within the range of soil denitrifying enzyme activity (0–100 μg N kg^{-1} h^{-1}) (Lu *et al.* 2022). The mean $\delta^{18}O$ values of soil water were between –10 and –6.5‰ (unpublished data from our group) at the initial interface of the denitrification zone in the soil profiles;

Table 1 Ranges of parameter values applied in the multi-process numerical model of dual NO_3^- isotope dynamics

Initial conditions	Description	Range	Reference
$[NO_3^-]_{initial}$	Initial $[NO_3^-]$	28.56–241.62 mg kg^{-1}	This study
$\delta^{15}N_{NO_3,\ initial}$	Initial $\delta^{15}N_{NO_3}$	–7.33–3.9‰	This study
$\delta^{18}O_{NO_3,\ initial}$	Initial $\delta^{18}O_{NO_3}$	–12.32–4.4‰	This study
$\delta^{18}O_{H_2O}$	$\delta^{18}O$ of ambient H_2O	–10–(–6.5)‰	This study
$^{15}\varepsilon_{NO3\ reduction}$	N isotope effect for NO_3^- reduction by denitrifiers	0–55‰	Buchwald and Wankel (2022) Granger *et al.* (2008)
$^{18}\varepsilon_{NO_3\ reduction}$	O isotope effect for NO_3^- reduction by denitrifiers	5–30‰	Asamoto *et al.* (2021)
$^{15}\varepsilon_{nxr}$	N isotope effect for NO_2^- oxidation by nitrifiers	–35–0‰	Kobayashi *et al.* (2019)
$^{18}\varepsilon_{nxr}$	O isotope effect for NO_2^- oxidation by nitrifiers	–8–(–1)‰	Casciotti (2009)
$^{18}\varepsilon_{nxrH_2O}$	O isotope effect for H_2O incorporation by nitrifiers	14‰	Buchwald and Casciotti (2010)
$^{18}\varepsilon_{eq}$	Equilibrium isotope effect between NO_2^- and H_2O	13.5‰	Buchwald and Casciotti (2013)
NRR	NO_3^- reduction by denitrifiers	0–100 μg N kg^{-1} h^{-1}	Lu *et al.* (2022)
NXR	NO_2^- oxidation by nitrifiers	0–100 μg N kg^{-1} h^{-1}	Lu *et al.* (2022)
R	Ratio of NO_2^- oxidation by nitrifiers to NO_3^- reduction by denitrifiers	0–0.95	Granger and Wankel (2016)

thus, the value of $\delta^{18}O_{NO_2}$ were ranging from 3.5 to 7‰ when $\delta^{18}O_{NO_2}$ reached equilibrium with $\delta^{18}O_{H_2O}$ in this model.

Apart from the measurable parameters and isotopic values, the isotopic effects involved in the process are all within a range of possible values. The inversion results of the model would introduce greater uncertainty. Therefore, we conducted an approach where each sampling point is inversely calculated with the initial interface of denitrification zone. This strategy simplifies the model and allows to more clearly analyze the process of NO_3^- reduction to NO_2^- and subsequent NO_2^- oxidation to NO_3^-, avoiding the complexity and interference caused by excessive parameter variations.

2.4. Functional gene quantification

DNA extraction DNA was extracted from 0.5 g of frozen slurry using the FastDNA™ Spin Kit for Soil (MP Biomedicals Southern California, USA), in accordance with the manufacturer's protocols. The quality of extracted DNA was evaluated by 1% agarose gel electrophoresis; DNA concentrations and purity were checked using a bistable timing electrophoresis apparatus and spectrophotometer.

Functional gene quantification The abundances of the *narG*, *napA*, and *nxrA* genes encoding NO_3^- reductase and NO_2^- oxidoreductase in soil slurries were quantified *via* quantitative polymerase chain reaction (qPCR) with an ABI7300 Thermal Cycler PCR thermocycler (Applied Biosystems, USA). qPCR was performed by Majorbio Bio-Pharm Technology (Shanghai, China). The *narG* gene fragment (627 bp) was amplified using primers *narG*145F (5′-ACSCAYGGSGTDAACTGYAC-3′) and *narG*733r (5′-GGNACGTTNGADCCCCA-3′); the thermocycler conditions were an initial 3 min at 95°C, followed by 40 cycles of 95°C for 5 s, 58°C for 30 s, and 72°C for 1 min. The *napA* gene fragment (130 bp) was amplified using primers *napA*-3F (5′-CCCAATGCTCGCCACTG-3′) and *napA*-3R (5′-CATGTTKGAGCCCCACAG-3′); the thermocycler conditions were an initial 3 min at 95°C, followed by 40 cycles of 95°C for 5 s, 58°C for 30 s, and 72°C for 1 min. The *nxrA* gene fragment (323 bp) was amplified using primers F1norA (5′-CAGACCGACGTGTGCGAAAG-3′) and R1norA (5′-TCYACAAGGAACGGAAGGTC-3′ (Y=C or T); the thermocycler conditions were an initial 3 min at 95°C, followed by 40 cycles of 95°C for 5 s, 58°C for 30 s, and 72°C for 1 min.

PCR products were purified using a kit developed by Majorbio Bio-Pharm Technology (Shanghai, China). qPCR mixtures (20 μL) contained 10 μL of 2× ChamQ SYBR Color qPCR Master Mix, 0.8 μL of primer F (5 μmol L^{-1}), 0.8 μL of primer R (5 μmol L^{-1}), 0.4 μL of 50× ROX Reference Dye 1, 2 μL of template DNA, and 6 μL of ddH_2O. Standard qPCR curves were obtained from serial 10-fold dilutions of plasmid DNA carrying the target gene inserts. Each sample was quantified in triplicate, and sterile water was used as a negative control. The mean specific qPCR primer set amplification efficiency was 102%, and R^2 of the standard curve was >0.98.

2.5. Metabolomics analyses

Metabolites were extracted using a solution (methanol: water=4:1 (v:v)) containing 0.02 mg mL^{-1} internal standard (L-2-chlorophenylalanine). Six replicates were established for soil samples from the $\Delta\delta^{18}O$:$\Delta\delta^{15}N$ trajectory groups. A quality control sample was inserted every 5–15 samples to confirm analytical stability. Liquid chromatography–tandem mass spectrometry (LC-MS/MS) analysis of the samples was conducted on a Thermo UHPLC-Q Exactive HF-X system equipped with an ACQUITY HSS T3 column (100 mm×2.1 mm i.d., 1.8 μm; Waters Corporation, Milford, MA, USA) at Majorbio Bio-Pharm Technology. The spectrometer was equipped with an electrospray ionization source operating in positive and negative ion modes.

2.6. Statistical analysis

Soil properties, the values of $\delta^{15}N$- and $\delta^{18}O$-NO_3^-, output results of the multi-process numerical model of dual NO_3^- isotope dynamics, and functional gene copy number data were subjected to one-way analysis of variance or Pearson correlation analysis in IBM SPSS 25.0 software. Statistically significant differences were determined using a *P*-value threshold of less than 0.05 unless otherwise stated.

Raw LC-MS/MS data were pre-processed using Progenesis QI software (Waters Corporation, Milford, USA), and a three-dimensional data matrix in CSV format was exported. Metabolites were identified using HMDB (http://www.hmdb.ca/), Metlin (https://metlin.scripps.edu/), and Majorbio databases. The data matrix was pre-processed through the Majorbio cloud platform (cloud.majorbio.com) to obtain final data for analyses. Then, the "ropls" package (ver. 1.6.2) in R software was used to perform principal component analysis (PCA) and orthogonal partial least squares discriminant analysis (OPLS-DA), as well as 200-cycle interactive validation evaluating model stability. Metabolites with variable importance in projection (VIP) value>1 and *P*-value<0.05 were considered significantly different based on VIP values obtained by OPLS-DA and *P*-value generated by Student's *t*-test.

3. Results

3.1. Physicochemical properties

The physicochemical properties of the sampling sites exhibit spatial variation and vary with depth profile (Appendix A). Of the soil quality parameters assessed, the pH ranged from 7.19 to 9.81, salinity ranged from 0.19 to 3.69 g kg^{-1}, NH_4^+ content ranged from 0.01 to 0.45 mg kg^{-1}, and NO_2^- content ranged from 0.01 to 2.37 mg kg^{-1}. The soil samples had TN contents ranging from 0.09 to 1.38 g kg^{-1} and SOC contents ranging from 1.26 to 17.65 g kg^{-1}.

3.2. Nitrate contents, $\delta^{15}N$- and $\delta^{18}O$-NO_3^-, and the $\Delta\delta^{18}O$:$\Delta\delta^{15}N$ trajectory

The NO_3^- contents at all sampling sites decreased according to the soil profile (Fig. 2), indicating NO_3^- attenuation. The minimum NO_3^- content decreased by up to 4.07 mg kg^{-1} (Fig. 2-A), while the maximum NO_3^- content increased by up to 241.62 mg kg^{-1} (Fig. 2-B). The $\delta^{15}N$-NO_3^- values ranged from –7.33 to 16.77‰, whereas the $\delta^{18}O$-NO_3^- values ranged from –18.79 to 16.41‰. Both $\delta^{15}N$- and $\delta^{18}O$-NO_3^- values

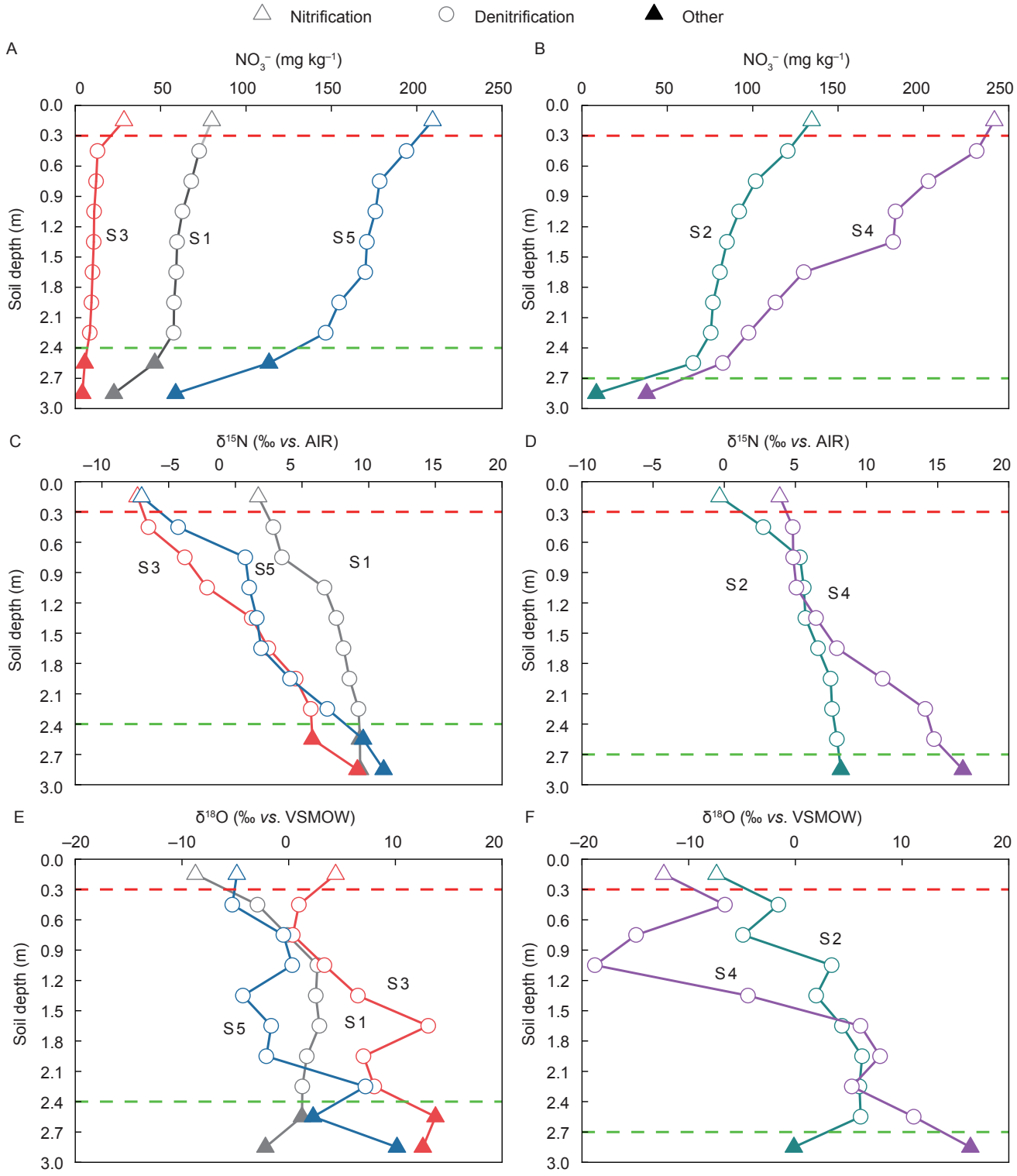


Fig. 2 Variation in NO_3^- contents and $\delta^{15}N$- and $\delta^{18}O$-NO_3^- values across soil profiles at the sampling sites. The sampling sites are labeled S1 through S5. The standard reference materials employed were the atmospheric nitrogen standard for nitrogen isotope analysis (AIR) and the Vienna standard mean ocean water (VSMOW).

showed an increasing trend along soil profiles (Fig. 3).

Each sampling site was divided into three zones according to NO_3^- content and $\delta^{15}N$ variation (Figs. 2 and 3): nitrification, denitrification, and other. The nitrification zone mainly occurred in topsoil, where NO_3^- was produced through exogenous inputs or nitrification and had a low $\delta^{15}N$ (Wang *et al.* 2018); the denitrification zone was predicted by the Rayleigh model, where there were significant linear relationships between $\delta^{15}N$-NO_3^- values according to the natural logarithm of the fraction of remaining NO_3^- (the slope is the apparent N isotope effect, $^{15}\varepsilon_{app}$) (Zhan *et al.* 2024); NO_3^- attenuation was observed in the other zone without

typical isotope effects, which might be mainly affected by uncertain specific processes, rather than denitrification, and requires further study. The denitrification zone was the dominant NO_3^- attenuation area. For the five sampling points, $\delta^{15}N$-NO_3^- was significantly negatively correlated with SOC and NO_3^- (P<0.05) (Appendices B–F). In denitrification, NO_3^- is the substrate and SOC is the main electron donor; consumption of the two is conducive to denitrification (Wunderlich *et al.* 2012). Environmental variables such as pH and salinity did not significantly differ among sampling sites and were within the range of denitrifying bacteria activity; thus, they were not considered main influencing factors of denitrification warranting further investigation.

In contrast, the $\delta^{15}N$- and $\delta^{18}O$-NO_3^- values of the denitrification zones were positively correlated (P<0.05) at all sampling sites (Fig. 3). The $\Delta\delta^{18}O$:$\Delta\delta^{15}N$ trajectories varied from 0.53 to 2.24 and fell into two groups: below 1 (0.53, 0.78, and 0.92 for S1, S3, and S5, respectively) and above 1 (1.57 and 2.24 for S2 and S4, respectively). Two $\Delta\delta^{18}O$:$\Delta\delta^{15}N$ trajectory types were observed in areas both affected and unaffected by seawater intrusion and regression. For the group with $\Delta\delta^{18}O$:$\Delta\delta^{15}N$ trajectories below 1, $^{15}\varepsilon_{app}$ was greater than 25‰ (27.71, 30.00, and 35.96‰ for S1, S3, and S5, respectively), whereas it was less than 25‰ (8.43 and 10.70‰ for S2 and S4, respectively) for the group with $\Delta\delta^{18}O$:$\Delta\delta^{15}N$ trajectories above 1.

3.3. Isotope effects and NO_2^- oxidation ratios of the $\Delta\delta^{18}O$:$\Delta\delta^{15}N$ trajectory groups below and above 1

The output of the multi-process numerical model of dual NO_3^- isotope dynamics significantly differed between the two groups with $\Delta\delta^{18}O$:$\Delta\delta^{15}N$ trajectories below and above 1 (Fig. 4). In the group with $\Delta\delta^{18}O$:$\Delta\delta^{15}N$ trajectories below 1, the NO_2^- oxidation ratio (R) ranged from 0 to 0.9, which was wider than the range of 0.2 to 0.5 for the group with the $\Delta\delta^{18}O$:$\Delta\delta^{15}N$ trajectories above 1; the mean value in the

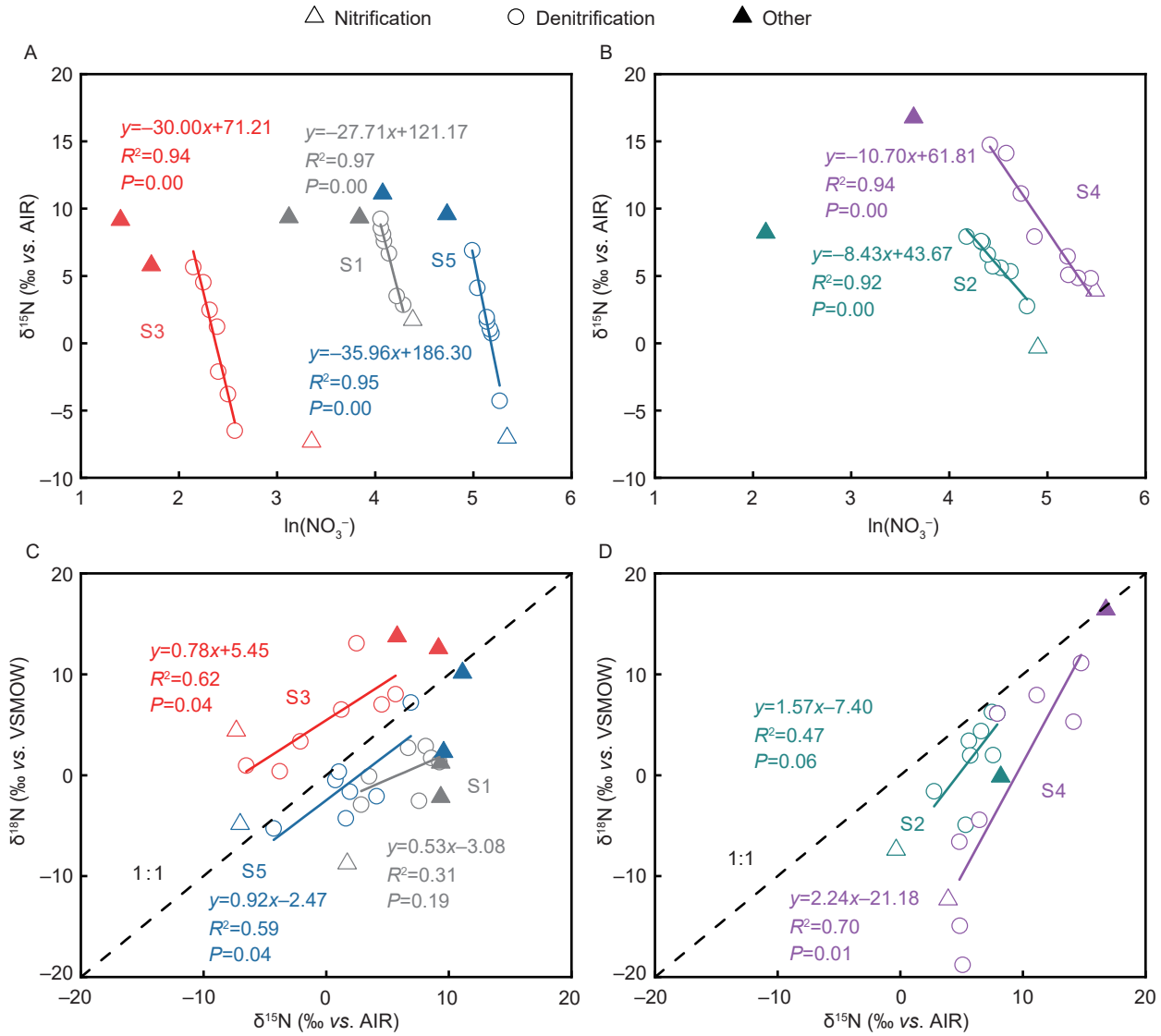


Fig. 3 Apparent N isotope effects ($^{15}\varepsilon_{app}$) and $\Delta\delta^{18}O$:$\Delta\delta^{15}N$ trajectories at different sampling sites. The sampling sites are labeled S1 through S5. The standard reference materials employed were the atmospheric nitrogen standard for nitrogen isotope analysis (AIR) and the Vienna standard mean ocean water (VSMOW).

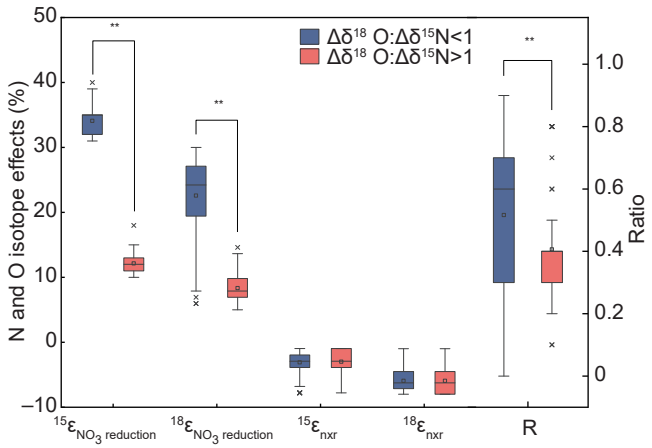


Fig. 4 Isotope effects and NO_2^- oxidation ratios of the two $\Delta\delta^{18}O$:$\Delta\delta^{15}N$ trajectory groups simulated by the multi-process numerical model of dual NO_3^- isotope dynamics. $^{15}\varepsilon_{NO3\ reduction}$, N isotope effect on NO_3^- reduction by denitrifiers; $^{18}\varepsilon_{NO3\ reduction}$, O isotope effect on NO_3^- reduction by denitrifiers; $^{15}\varepsilon_{nxr}$, N isotope effect on NO_2^- oxidation by nitrifiers; $^{18}\varepsilon_{nxr}$, O isotope effect on NO_2^- oxidation by nitrifiers; R, NO_2^- oxidation ratio. Error bar is SD (n=50). **, P<0.01.

former group (0.52±0.22) was significantly higher than that in the latter group (0.34±0.09).

The group with $\Delta\delta^{18}O$:$\Delta\delta^{15}N$ trajectories below 1 also had a wider range (31.0–39.0‰) and significantly higher mean value (34.07±1.96‰) of $^{15}\varepsilon_{NO3\ reduction}$ compared with the other group (range: 10–15‰, mean: 12.02±1.39‰). The isotope effects of $^{18}\varepsilon_{NO3\ reduction}$ ranged from 7.88 to 30‰ in the group with $\Delta\delta^{18}O$:$\Delta\delta^{15}N$ trajectories below 1 and from 5 to 13.65‰ in the group with $\Delta\delta^{18}O$:$\Delta\delta^{15}N$ trajectories above 1; the mean value was significantly higher in the former group (22.83±5.46‰ *vs*. 8.22±2.11‰). The isotope effects of $^{15}\varepsilon_{nxr}$ were similar to those of $^{18}\varepsilon_{nxr}$ in both groups: $^{15}\varepsilon_{nxr}$ range: –6.81 to –0.97‰ (mean: –2.97±1.78‰) and $^{18}\varepsilon_{nxr}$ range: –8.0 to –1.0‰ (mean: –5.93±1.94‰) in the group with $\Delta\delta^{18}O$:$\Delta\delta^{15}N$ trajectories below 1; range: –7.78 to –0.97‰ (mean: –2.99±2.00‰) for $^{15}\varepsilon_{nxr}$ and range: –8 to –1‰ (mean: –5.94±1.97‰) for $^{18}\varepsilon_{nxr}$ in the group with $\Delta\delta^{18}O$:$\Delta\delta^{15}N$ trajectories above 1.

In the correlation analysis of the model output (Tables 2 and 3), $^{15}\varepsilon_{NO3\ reduction}$ was significantly positively correlated with $^{15}\varepsilon_{nxr}$ and R, whereas $^{15}\varepsilon_{nxr}$ was significantly positively correlated with $^{18}\varepsilon_{nxr}$ in both groups.

3.4. Functional genes (*narG*, *napA*, and *nxrA*) encoding NO_3^- reductase and NO_2^- oxidoreductase in the $\Delta\delta^{18}O$:$\Delta\delta^{15}N$ trajectory groups below and above 1

The *narG*, *napA*, and *nxrA* genes encoding NO_3^- reductase and NO_2^- oxidoreductase had 1.05×10^7, 9.13×10^6, and 5.35×10^5 copies g^{-1}, respectively, in the group with $\Delta\delta^{18}O$:$\Delta\delta^{15}N$ trajectories below 1, and 4.64×10^6, 3.36×10^6, and 3.06×10^4 copies g^{-1} in the group with $\Delta\delta^{18}O$:$\Delta\delta^{15}N$ trajectories above 1 (Appendix G). The copy numbers of all three functional genes were significantly higher in the group with $\Delta\delta^{18}O$:$\Delta\delta^{15}N$ trajectories below 1. There was a positive correlation between the *narG* gene copy number and the copy numbers of *napA* and *nxrA* genes in both groups, whereas there was no significant correlation between *napA* and *nxrA* (Fig. 5).

Table 2 Correlation analysis of isotope effects and NO_2^- oxidation ratios simulated by the multi-process numerical model of dual NO_3^- isotope dynamics for the group with $\Delta\delta^{18}O$:$\Delta\delta^{15}N$ trajectories below 1[1)]

	$^{15}\varepsilon_{NO3\ reduction}$	$^{18}\varepsilon_{NO3\ reduction}$	$^{15}\varepsilon_{nxr}$	$^{18}\varepsilon_{nxr}$	R
$^{15}\varepsilon_{NO3\ reduction}$	1	–0.043	0.308**	–0.063	0.456**
$^{18}\varepsilon_{NO3\ reduction}$		1	–0.055	0	–0.220
$^{15}\varepsilon_{nxr}$			1	0.475**	–0.015
$^{18}\varepsilon_{nxr}$				1	0.044
R					1

1) $^{15}\varepsilon_{NO3\ reduction}$, the N isotope effect on NO_3^- reduction by denitrifiers; $^{18}\varepsilon_{NO3\ reduction}$, the O isotope effect on NO_3^- reduction by denitrifiers; $^{15}\varepsilon_{nxr}$, the N isotope effect on NO_2^- oxidation by nitrifiers; $^{18}\varepsilon_{nxr}$, the O isotope effect on NO_2^- oxidation by nitrifiers; R, NO_2^- oxidation ratios.
*, P<0.05; **, P<0.01.

Table 3 Correlation analysis of the isotope effects and NO_2^- oxidation ratios simulated by the multi-process numerical model of dual NO_3^- isotope dynamics for the group with $\Delta\delta^{18}O$:$\Delta\delta^{15}N$ trajectories above 1[1)]

	$^{15}\varepsilon_{NO3\ reduction}$	$^{18}\varepsilon_{NO3\ reduction}$	$^{15}\varepsilon_{nxr}$	$^{18}\varepsilon_{nxr}$	R
$^{15}\varepsilon_{NO3\ reduction}$	1	0.318	0.444**	–0.228	.662**
$^{18}\varepsilon_{NO3\ reduction}$		1	–0.390	–0.198	–0.043
$^{15}\varepsilon_{nxr}$			1	0.540**	–0.197
$^{18}\varepsilon_{nxr}$				1	0
R					1

1) $^{15}\varepsilon_{NO3\ reduction}$, the N isotope effect on NO_3^- reduction by denitrifiers; $^{18}\varepsilon_{NO3\ reduction}$, the O isotope effect on NO_3^- reduction by denitrifiers; $^{15}\varepsilon_{nxr}$, the N isotope effect on NO_2^- oxidation by nitrifiers; $^{18}\varepsilon_{nxr}$, the O isotope effect on NO_2^- oxidation by nitrifiers; and R, NO_2^- oxidation ratios.
*, P<0.05; **, P<0.01.

3.5. Carbon sources from metabolites in the $\Delta\delta^{18}O$:$\Delta\delta^{15}N$ trajectory groups below and above 1

There was a significant relationship between the isotopic values of ^{15}N-NO_3^- and the SOC content (Appendices B–F); a study conducted in the same areas indicated that the dominant organic carbon source was derived from microorganisms (Leng *et al.* 2023). An untargeted metabolomics approach was used to analyze the metabolites in the $\Delta\delta^{18}O$:$\Delta\delta^{15}N$ trajectory groups below and above 1, as well as the differences in metabolites between the two groups. In total, 471 metabolites were detected in positive and negative modes; PCA showed that the metabolites differed between the two $\Delta\delta^{18}O$:$\Delta\delta^{15}N$ trajectory groups (Appendix H-a and b). The results of supervised OPLS-DA showed significant separation between the two groups and clustering within the groups (Appendix H-c and d). The values of R^2Y and Q^2 of OPLS-DA permutation testing (Appendix H-e and f) were close to 1, indicating that the model was stable and reliable.

Of the 471 metabolites, 42 could be used as carbon sources for denitrification and belonged to nine groups of compounds according to the Human Urine Metabolome

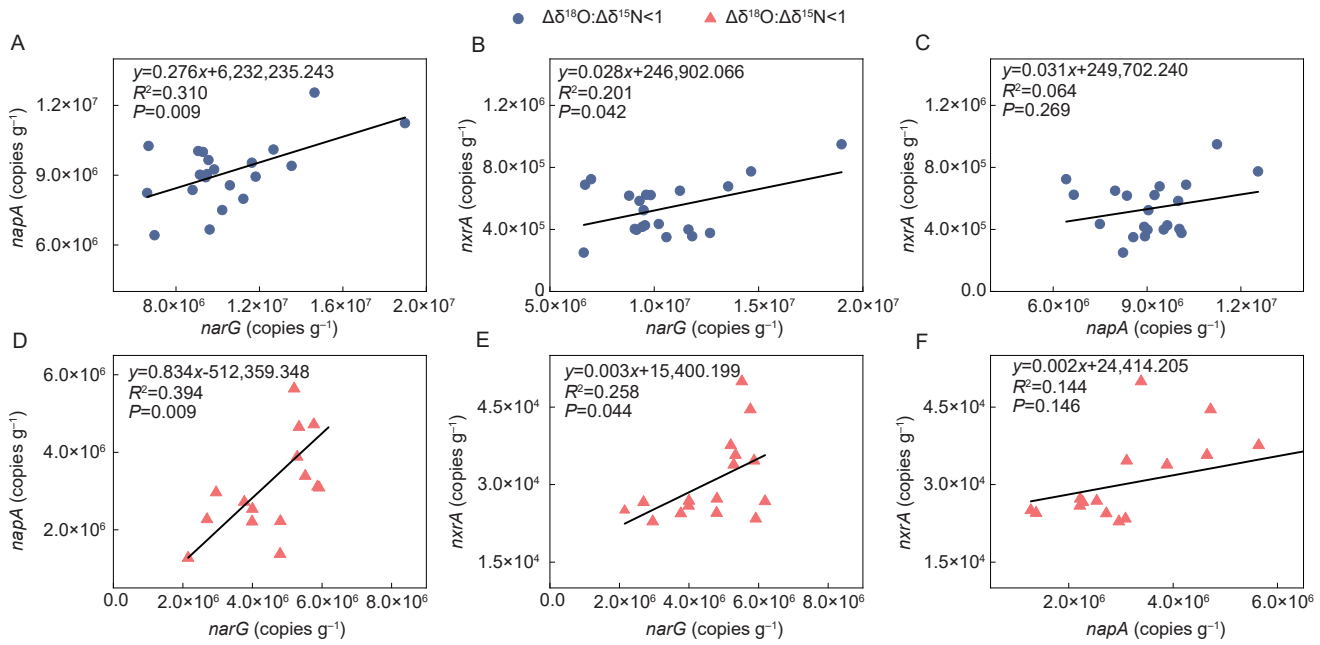


Fig. 5 Correlations among the copy numbers of functional genes encoding NO_3^- reductase (*narG* and *napA*) and NO_2^- oxidoreductase (*nxrA*) in the two $\Delta\delta^{18}O$:$\Delta\delta^{15}N$ trajectory groups.

Database (HMDB) (http://www.urinemetabolome.ca/) (Appendix I). Of the carbon sources, 81% belonged to lipids and lipid-like molecules, organoheterocyclic compounds, organic acids and derivatives, and benzenoids.

Of the 42 metabolites, the expression patterns of 16 significantly differed between the two groups (VIP>1, P<0.05) (Fig. 6): 11 metabolites in the group with $\Delta\delta^{18}O$:$\Delta\delta^{15}N$ trajectories below 1 were upregulated (2-methylpyridine, homogentisic acid, lactic acid, L-phenylalanine, guanine, vanillin, hypoxanthine, trehalose, propionic acid, butyric acid, and cyclohexanecarboxylic acid), whereas five metabolites in the group with $\Delta\delta^{18}O$:$\Delta\delta^{15}N$ trajectories above 1 were upregulated (palmitic acid, urocanic acid, 4-nitrophenol, morpholine, and phthalic acid).

4. Discussion

4.1. Comparison of isotope effects and NO_2^- oxidation ratios between the two $\Delta\delta^{18}O$:$\Delta\delta^{15}N$ trajectory groups

In simulations conducted using the multi-process numerical model of dual NO_3^- isotope dynamics (Granger and Wankel 2016), the two $\Delta\delta^{18}O$:$\Delta\delta^{15}N$ trajectory groups had similarities (Tables 2 and 3) and significant differences in $^{15}\varepsilon_{NO_3\ reduction}$, $^{18}\varepsilon_{NO_3\ reduction}$, $^{15}\varepsilon_{nxr}$, $^{18}\varepsilon_{nxr}$, and R (Fig. 4). In both $\Delta\delta^{18}O$:$\Delta\delta^{15}N$ trajectory groups, the increase in $^{15}\varepsilon_{NO_3\ reduction}$ enhanced the inverse isotope effect of NO_2^- oxidation ($^{15}\varepsilon_{nxr}$) and the NO_2^- oxidation ratio (R) (Tables 2 and 3). Typically, greater $^{15}\varepsilon_{NO_3\ reduction}$ is associated with a higher rate of cell-specific NO_3^- reduction to NO_2^- (Kritee *et al.* 2012). In this study, $^{15}\varepsilon_{NO_3\ reduction}$ was significantly higher in the group with $\Delta\delta^{18}O$:$\Delta\delta^{15}N$ trajectories below 1 (Fig. 4), indicating a higher rate of NO_3^- reduction. Moreover, the copy numbers of the *narG*, *napA*, and *nxrA* genes were also higher in the group with $\Delta\delta^{18}O$:$\Delta\delta^{15}N$ trajectories below 1 than in the other group (Appendix G), which was more conductive to NO_3^- reduction. Consequently, the NO_2^- contents in the instantaneous NO_2^- pools were relatively higher in the group with $\Delta\delta^{18}O$:$\Delta\delta^{15}N$ trajectories below 1 and promoted the oxidation of NO_2^- to NO_3^- (Fig. 4) or NO_2^- reduction. However, the isotope effects of $^{15}\varepsilon_{nxr}$ and $^{18}\varepsilon_{nxr}$ in both groups were in a similar range and require further investigation.

Furthermore, the simulated range of $^{15}\varepsilon_{NO_3\ reduction}$ (31.0–39.0‰) in the group with $\Delta\delta^{18}O$:$\Delta\delta^{15}N$ trajectories below 1 exceeded the reported isotope effect range of Nar reductase (6.6–31.6‰), implying the involvement of other NO_3^- reductases that can reduce NO_3^- to NO_2^- (Asamoto *et al.* 2021). As reported, the isotope effects of Nap reductase ranged from 11.4 to 39.8‰ (Treibergs and Granger 2017), similar to the maximum value simulated by the model. Based on the similar structures and regulatory mechanisms of Nar reductase and Nxr oxidoreductase, Nxr oxidoreductase can also catalyze the reduction of NO_3^-, causing the N isotope effect to reach 55‰ (Buchwald and Wankel 2022). Therefore, the simulated $^{15}\varepsilon_{NO_3\ reduction}$ values suggest a combined effect of multiple NO_3^- reductases in the group with $\Delta\delta^{18}O$:$\Delta\delta^{15}N$ trajectories below 1. The positive relationship between the copy numbers of *narG* and those of *napA* and *nxrA* was consistent with this conclusion (Fig. 5). In the group with $\Delta\delta^{18}O$:$\Delta\delta^{15}N$ trajectories above 1, multiple NO_3^- reductases were also involved (*narG*, *napA*, and *nxrA*). This involvement may contribute to the lack of a significant correlation between $^{15}\varepsilon_{NO_3\ reduction}$ and $^{18}\varepsilon_{NO_3\ reduction}$ in the present study (Tables 2 and 3) due to the specific isotope effects of each NO_3^- reductase. In contrast, under anaerobic or anoxic conditions, the oxidation of NO_2^- to NO_3^- is only catalyzed by Nxr and $^{15}\varepsilon_{nxr}$ was significantly correlated with $^{18}\varepsilon_{nxr}$ (Tables 2 and 3).

In conclusion, $^{15}\varepsilon_{NO_3\ reduction}$, $^{18}\varepsilon_{NO_3\ reduction}$, the NO_2^- oxidation ratio, and the *narG*, *napA*, and *nxrA* copy numbers were

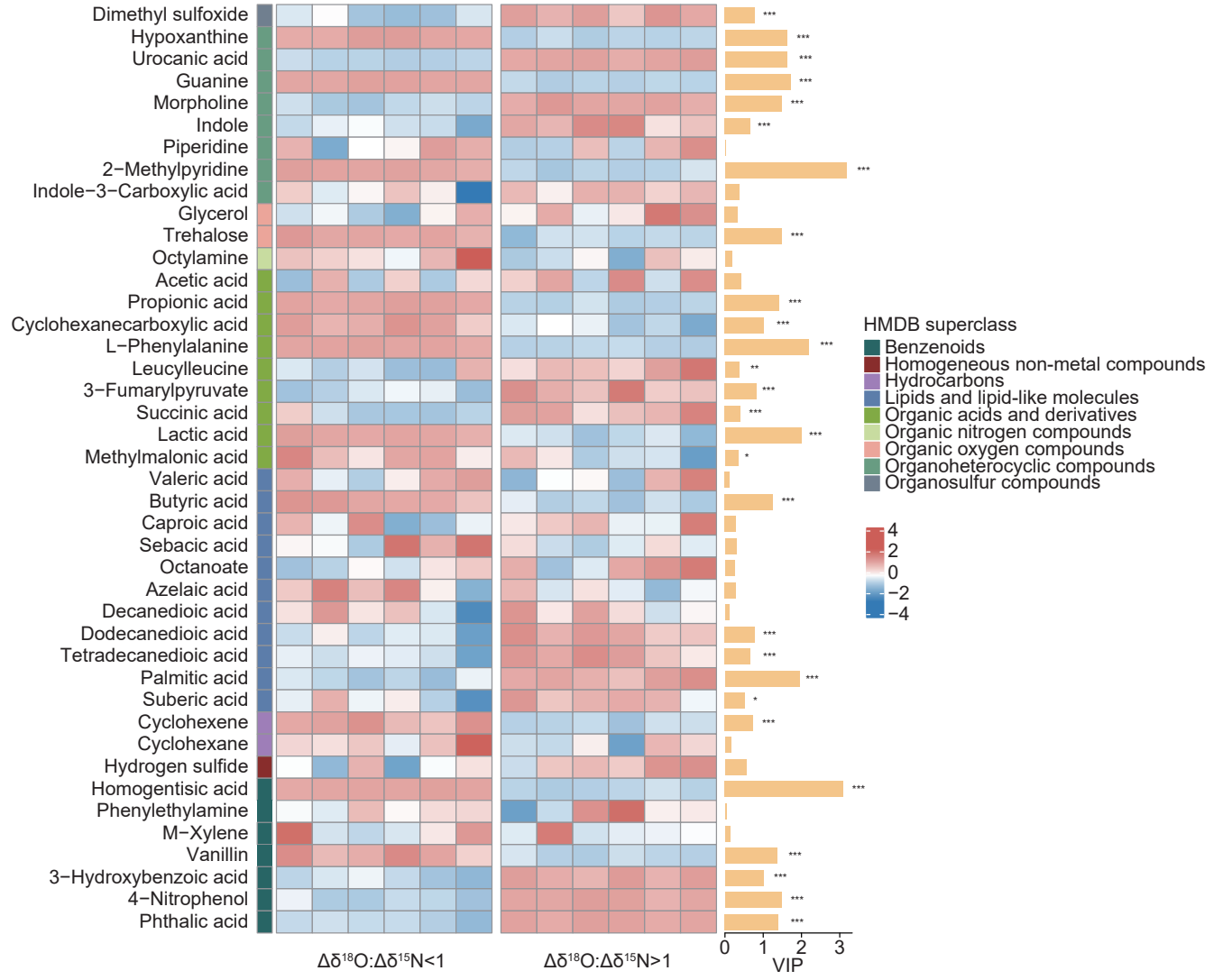


Fig. 6 Heatmap of carbon sources from metabolites in the two $\Delta\delta^{18}O$:$\Delta\delta^{15}N$ trajectory groups. Unpaired Student's *t*-tests were performed with OPLS-DA to identify discrepant metabolites. The *P*-values for Student's *t*-test and variable importance in projection (VIP) values for the OPLS-DA model are shown. *, $P<0.05$; **, $P<0.01$; ***, $P<0.001$.

significantly higher in the group with $\Delta\delta^{18}O$:$\Delta\delta^{15}N$ trajectories below 1 than in the other group (Fig. 4 and Appendix G). Therefore, at the cellular level, NO_3^- reduction to NO_2^- was more active in the group with $\Delta\delta^{18}O$:$\Delta\delta^{15}N$ trajectories below 1. Moreover, the difference in $^{15}\varepsilon_{NO_3\ reduction}$ and $^{18}\varepsilon_{NO_3\ reduction}$ between the two groups was significant, whereas the difference between $^{15}\varepsilon_{nxr}$ and $^{18}\varepsilon_{nxr}$ was the minimal. Therefore, the reduction of NO_3^- to NO_2^- has a more substantial effect on the $\Delta\delta^{18}O$:$\Delta\delta^{15}N$ trajectories and it is important to study the factors influencing NO_3^- reduction to NO_2^-, which may provide electrons and energy for this process and affect the up- or downregulation of corresponding genes that result in N and O isotopic fractionation as the bonds of NO_3^- break and form.

4.2. Other N transformation processes and factors influencing the two $\Delta\delta^{18}O$:$\Delta\delta^{15}N$ trajectory groups

In NO_3^- consuming systems, other concurrent N processes and factors (e.g., diffusion limitation substrate limitation and etc.) can simultaneously mediate the production and reduction of NO_3^-, modulating the characteristic slope ($\Delta\delta^{18}O$:$\Delta\delta^{15}N$) observed in isotopic enrichment trajectories.

Primary NO_3^- production pathways include anaerobic ammonium oxidation (anammox), a chemoautotrophic process coupling NH_4^+ oxidation to N_2 with NO_2^- reduction under anoxic conditions, which stoichiometrically produces ~0.26 moles of NO_3^- per mole of NH_3 oxidized (or per 1.3 moles of NO_2^- reduced) (Van de Graaf *et al.* 1995; Strous *et al.* 1999; Jetten *et al.* 2009). The N and O isotope effects associated with anammox metabolism has been reported in only a few studies, which showed inverse N kinetic isotope effects ranging from −45.3 to −30.1‰ (Brunner *et al.* 2013; Kobayashi *et al.* 2019) and from –77.8 to –65.9‰ (Kobayashi *et al.* 2019). Since the reduction of NO_3^- to N_2 and the oxidation of NO_2^- occur simultaneously in the anammox process, there is a lack of detailed information on isotopic fractionation for the NO_2^- oxidation. Moreover, the actual subcellular localization and amino acid sequences of enzymes in anammox bacteria are not fully understood,

thus influence on N and O isotope effects need to be further investigated (Kobayashi *et al.* 2019).

NO_3^- reduction to NO_2^- occurs *via* three key anaerobic pathways: denitrification, dissimilatory nitrate reduction to ammonium (DNRA) (Lam and Kuypers 2011), and nitrate-dependent anaerobic oxidation of methane (nitrate-dependent AOM) (Welte *et al.* 2016). Denitrification and DNRA are catalyzed by both membrane-bound (Nar) and periplasmic (Nap) NO_3^- reductases, while nitrate-dependent AOM exclusively utilizes Nar-type enzymes (Arshad *et al.* 2015; Treibergs and Granger 2017). The denitrification zone in this study was predominantly inhabited by denitrifying bacteria, very little component of DNRA bacteria, and with no detectable levels of anammox or nitrate-dependent AOM observed (unpublished data). Notably, the consistently low NH_4^+ concentrations (Appendix A) and absence of its accumulation within the denitrification zone suggest that the $\Delta\delta^{18}O$:$\Delta\delta^{15}N$ trajectory is primarily controlled by denitrification process.

Effects of diffusion limitation and substrate limitation may modulate the $\Delta\delta^{18}O$:$\Delta\delta^{15}N$ trajectory. Under diffusion limitation, the slow transport rate of NO_3^- to reactive sites restricts NO_3^- reduction, resulting in an observed isotopic fractionation effect of 1.0–2.0‰ (Brandes and Devol 1997; Lehmann *et al.* 2004; Denk *et al.* 2017). In this study, the N isotopic effects (8.43–35.96‰) observed in both groups significantly exceed this range, which indicated that enzymatic activity dominates over diffusion limitation in governing NO_3^- isotopic fractionation. Additionally, substrate limitation of NO_3^- can influence its isotopic fractionation during reduction: when NO_3^- concentrations fall below the half-saturation constant (5–32 μmol L^{-1}) for NO_3^- transporters, insufficient substrate supply to maintain enzyme saturation reduces isotopic effects (Granger *et al.* 2008). However, the mean NO_3^- contents (11.35–157.19 mg kg^{-1} equivalent to 183.07–2,535.32 μmol L^{-1}) of denitrification zone in this study far exceed the range, which proved NO_3^- availability is not a limiting factor in the reduction process.

All five sampling sites demonstrated statistically significant negative correlations (P<0.05) between $\delta^{15}N$-NO_3^- and both SOC and NO_3^- contents (Appendices B–F). Furthermore, environmental parameters (e.g., pH and salinity) showed no significant spatial variation across sites, remaining within the optimal range for denitrifying bacterial activity. These observations suggest limited spatial heterogeneity impacts on denitrification processes. However, given the potential impact of spatiotemporal heterogeneity in soil profiles on denitrification dynamics, it is crucial to incorporate long-term monitoring coupled with multi-point sampling strategies in future investigations. Such comprehensive approaches would enable a systematic elucidation of how spatial distributions of soil physicochemical properties govern denitrification pathways and their associated isotopic fractionation mechanisms.

4.3. Comparison of factors influencing the two $\Delta\delta^{18}O$:$\Delta\delta^{15}N$ trajectory groups

Organic carbon is an important donor of electrons, which are essential for the reduction of NO_3^- to NO_2^- during denitrification (Pang and Wang 2021). In this study, approximately 38% of carbon sources from metabolites significantly differed between the two $\Delta\delta^{18}O$:$\Delta\delta^{15}N$ trajectory groups, which may have led to some differences in denitrification, especially in the isotope effects of the NO_3^- reduction and NO_2^- oxidation ratios.

More upregulated carbon sources with simple structures and low molecular weights, such as propionic, butyric, and lactic acids, were observed in the group with $\Delta\delta^{18}O$:$\Delta\delta^{15}N$ trajectories below 1 (Fig. 6). These substances have high electron production efficiency because they can enter the tricarboxylic acid cycle with minimal modification and undergo oxidation into the direct electron donor nicotinamide adenine dinucleotide (NADH) (Elefsiniotis *et al.* 2004; Su *et al.* 2019; Qi *et al.* 2021). The *narG* and *napA* genes for the NO_3^- reductases Nar and Nap both contain an active site with a molybdenum cofactor for NO_3^- catalysis and an iron-sulfur cluster as part of the electron transport chain (Coelho and Romao 2015). Thus, sufficient electrons are transported to active sites for rapid NO_3^- reduction (Wei *et al.* 2022). Other upregulated carbon sources in this group have high molecular weights and complex structures, such as 2-methylpyridine, phenylalanine, guanine, hypoxanthine, homogentisic acid, and cyclohexanecarboxylic acid. However, these substances can be degraded into small molecules, such as acetic, formic, and fumaric acids, which are readily used by denitrifying bacteria to promote NO_3^- reduction to NO_2^- (Rho and Evans 1975; Bollag and Kaiser 1991; Schneider *et al.* 1997; Wang *et al.* 2009; Mekala *et al.* 2019; Chen *et al.* 2023). In the group with $\Delta\delta^{18}O$:$\Delta\delta^{15}N$ trajectories below 1, we found that vanillin was used as both a carbon source and a quorum-sensing inhibitor. Quorum sensing (QS) regulates nitrification *via* signaling molecules such as N-acyl homoserine lactones (AHLs), which enhance ammonia monooxygenase (AMO) activity in ammonia-oxidizing bacteria (AOB) while suppressing NO_2^- oxidoreductase (Nxr) in nitrite-oxidizing bacteria (NOB), thereby limiting NO_2^- oxidation to NO_3^- (Ruan *et al.* 2020; Chen *et al.* 2023). However, vanillin attenuates AHL-mediated QS and stimulates Nxr activity (Chen *et al.* 2023). Furthermore, vanillin serves as an exogenous carbon source that stimulates denitrifier proliferation, thereby modulating nitrogen metabolic pathways (Brozinčević *et al.* 2024). Notably, upregulated vanillin-associated expression in the group with $\Delta\delta^{18}O$:$\Delta\delta^{15}N$ trajectory less than 1 (Fig. 6) highlights its dual role in enhancing NO_3^- reduction and NO_2^- oxidation *via* Nxr activation. Such inhibitors serve as signaling molecules to improve Nxr oxidoreductase activity and enhance its bidirectional function (Chen *et al.* 2023). Some carbon sources also act as protective substances to maintain microbial activity under salinity stress, such as trehalose (Gregory and Boyd 2021). Therefore, the upregulated carbon sources from metabolites in this group favored the activities of the *narG*, *napA*, and *nxrA* genes encoding NO_3^- reductase and NO_2^- oxidoreductase. These favored activities promote NO_3^- reduction to NO_2^- and enrich both ^{15}N and ^{18}O in the residual NO_3^-, resulting in stronger N and O isotope effects and higher NO_2^- oxidation ratios (Fig. 4). Conversely, the upregulated carbon sources in

the group with $\Delta\delta^{18}O$:$\Delta\delta^{15}N$ trajectories above 1 were either difficult to degrade because they had cyclic structures and high molecular weights (e.g., urocanic and phthalic acids) or were solids at room temperature (palmitic acid), causing inefficient electron generation and less efficient utilization by microorganisms (Chayabutra *et al.* 2001; Tomei and Annesini 2005; Jiang *et al.* 2017; Wang *et al.* 2023). Morpholine has a low molecular weight but exhibits a cyclic structure, which may enhance its degradation difficulty (Cech *et al.* 1988). Additionally, this group produced toxic compounds such as 4-nitrophenol. The upregulated carbon sources from metabolites in this group were not conducive to the genes encoding NO_3^- reductase and NO_2^- oxidoreductase.

The type of carbon source substance also affects NO_2^- accumulation. In the electron transport chain, electrons are more easily supplied to NO_3^- by coenzyme Q than to NO_2^- by cytochrome c; thus, NO_2^- tends to accumulate because NO_3^- reduction is faster than NO_2^- reduction (Ge *et al.* 2012; Wei *et al.* 2022). In this study, the NO_2^- content was much higher in the group with $\Delta\delta^{18}O$:$\Delta\delta^{15}N$ trajectories above 1 compared with the other group because the electron supply was relatively inefficient from carbon sources in the former group. Simultaneously, free nitrous acid, the ionized form of NO_2^-, can passively enter the plasma membranes of cells, reducing intracellular pH and inhibiting tricarboxylic acid carbon metabolism (Vadivelu *et al.* 2006; Zhou *et al.* 2011). This entry can affect the energy production of microorganisms and downregulate the expression of denitrifying reductases (Gao *et al.* 2016). Therefore, the copy numbers of functional genes, N and O isotope effects, and NO_2^- oxidation ratios were lower in the group with $\Delta\delta^{18}O$:$\Delta\delta^{15}N$ trajectories above 1.

NO_3^- is the electron acceptor in the denitrification process; thus, Nar and Nap reductases compete for it. In the present study, the NO_3^- content was not the limiting factor for NO_3^- reduction to NO_2^-. The discovery of a synergistic effect of multiple functional genes (*narG*, *napA*, and *nxrA*) was intriguing. Nar reductase, involved in respiration, is ubiquitous in denitrifying microbe communities. The Nar operon is conserved and upregulated under anaerobic conditions, as well as by the presence of NO_3^- (González *et al.* 2006). However, the Nap operon is much less conserved and can incorporate various genes from other microbes (Richardson *et al.* 2001; Kraft *et al.* 2011; Sparacino-Watkins *et al.* 2014; Asamoto *et al.* 2021). Unsaturated zone soils possess a large range of redox gradients within a few centimeters; they also experience extensive changes in moisture and oxygen on short time scales, thereby connecting the NO_3^- affinity of Nar *vs*. Nap to environmental constraints. The complexity and flexibility of Nap regulation may reduce competition with Nar. The bidirectional functions of Nxr oxidoreductase should also promote cooperation to reduce NO_3^- and oxidize NO_2^- in the environment.

Various carbon sources affect the efficiency of electron production, the competition of reductases for electrons, and the consumption and accumulation of NO_2^- during denitrification. These factors affect the activities of the genes encoding NO_3^- reductase and NO_2^- oxidoreductase, thereby influencing the N and O isotope effects of NO_3^- and NO_2^- oxidation ratios in the two $\Delta\delta^{18}O$:$\Delta\delta^{15}N$ trajectory groups. Further research is needed to determine how Nar, Nap, and Nxr cooperate and compete in the presence of different carbon sources to influence variation in the $\Delta\delta^{18}O$:$\Delta\delta^{15}N$ trajectory.

5. Conclusion

This study showed that NO_3^- reduction was more important for the $\Delta\delta^{18}O$:$\Delta\delta^{15}N$ trajectory variation because the difference in isotope effects ($^{15}\varepsilon_{NO_3\ reduction}$ and $^{18}\varepsilon_{NO_3\ reduction}$) between the two groups was significant, whereas the difference in isotope effects ($^{15}\varepsilon_{nxr}$ and $^{18}\varepsilon_{nxr}$) upon NO_2^- oxidation was not. This study revealed the integrated influence of the isotope effects, activities of NO_3^- reductase and NO_2^- oxidoreductase, and carbon sources from metabolites. These findings represent an important step toward a comprehensive understanding of the $\Delta\delta^{18}O$:$\Delta\delta^{15}N$ trajectories for N cycling identification in terrestrial ecosystems. It also provides critical insights for groundwater protection through optimized carbon amendment strategies that enhance microbial NO_3^- reduction while enabling $\Delta\delta^{18}O$:$\Delta\delta^{15}N$-based monitoring of denitrification efficiency in terrestrial ecosystems.

Acknowledgements

This work was financially supported by the National Natural Science Foundation of China (42361144860, 41973017 and 32071861).

Declaration of competing interest

The authors declare that they have no conflict of interest.

Declaration of generative AI and AI-assisted technologies in the writing process

The authors declare that they did not use AI in the preparation and writing of this manuscript.

Appendices associated with this paper are available at https://doi.org/10.1016/j.jia.2026.01.010

References

Arshad A, Speth D R, De Graaf R M, Op den Camp H J, Jetten M S, Welte C U. 2015. A metagenomics-based metabolic model of nitrate-dependent anaerobic oxidation of methane by *Methanoperedens*-like archaea. *Frontiers in Microbiology*, **6**, 1423.

Asamoto C K, Rempfert K R, Luu V H, Younkin A D, Kopf S H. 2021. Enzyme-specific coupling of oxygen and nitrogen isotope fractionation of the Nap and Nar nitrate reductases. *Environmental Science & Technology*, **55**, 5537–5546.

Bao Y F, Sun M, Wang Y C, Hu M M, Hu P, Wu L X, Huang W, Li S Z, Wen J, Wang Z J. 2024. Nitrate transformation and source tracking of Yarlung Tsangpo River using a multi-tracer approach combined with Bayesian stable isotope mixing model. *Environmental Research*, **252**, 118925.

Bollag J M, Kaiser J P. 1991. The transformation of heterocyclic aromatic compounds and their derivatives under anaerobic conditions. *Critical Reviews in Environmental Science Technology*, **21**, 297–329.

Böttcher J, Strebel O, Voerkelius S, Schmidt H L. 1990. Using isotope fractionation of nitrate-nitrogen and nitrate-oxygen for evaluation of microbial denitrification in a sandy aquifer. *Journal of Hydrology*, **114**, 413–424.

Brandes J A, Devol A H. 1997. Isotopic fractionation of oxygen and nitrogen in coastal marine sediments. *Geochimica et Cosmochimica*

Acta, **61**, 1793–1801.
Brozinčević A, Grgas D, Štefanac T, Habuda-Stanić M, Zelić B, Landeka Dragičević T. 2024. Cost reduction in the process of biological denitrification by choosing traditional or alternative carbon sources. *Energies*, **17**, 3660.
Brunner B, Contreras S, Lehmann M F, Matantseva O, Rollog M, Kalvelage T, Klockgether G, Lavik G, Jetten M S, Kartal B, Kuypers M M M. 2013. Nitrogen isotope effects induced by anammox bacteria. *Proceedings of the National Academy of Sciences of the United States of America*, **110**, 18994–18999.
Buchwald C, Casciotti K L. 2010. Oxygen isotopic fractionation and exchange during bacterial nitrite oxidation. *Limnology and Oceanography*, **55**, 1064–1074.
Buchwald C, Casciotti K L. 2013. Isotopic ratios of nitrite as tracers of the sources and age of oceanic nitrite. *Nature Geoscience*, **6**, 308–313.
Buchwald C, Santoro A E, Stanley R H R, Casciotti K L. 2015. Nitrogen cycling in the secondary nitrite maximum of the eastern tropical North Pacific off Costa Rica. *Global Biogeochemical Cycles*, **29**, 2061–2081.
Buchwald C, Wankel S D. 2022. Enzyme-catalyzed isotope equilibrium: A hypothesis to explain apparent N cycling phenomena in low oxygen environments. *Marine Chemistry*, **244**, 104–140.
Casciotti K L. 2009. Inverse kinetic isotope fractionation during bacterial nitrite oxidation. *Geochimica et Cosmochimica Acta*, **73**, 2061–2076.
Casciotti K L. 2016. Nitrogen and oxygen isotopic studies of the marine nitrogen cycle. *Annual Review of Marine Science*, **8**, 379–407.
Casciotti K L, Buchwald C, Mcilvin M. 2013. Implications of nitrate and nitrite isotopic measurements for the mechanisms of nitrogen cycling in the Peru oxygen deficient zone. *Deep Sea Research* (Part I: Oceanographic Research Papers), **80**, 78–93.
Casciotti K L, Sigman D M, Hastings M G, Böhlke J K, Hilkert A. 2002. Measurement of the oxygen isotopic composition of nitrate in seawater and freshwater using the denitrifier method. *Analytical Chemistry*, **74**, 4905–4912.
Cech J S, Hartman P, Slosárek M, Chudoba J. 1988. Isolation and identification of a morpholine-degrading bacterium. *Applied & Environmental Microbiology*, **54**, 619–621.
Chayabutra C, Wu J, Ju L K. 2001. Rhamnolipid production by *Pseudomonas aeruginosa* under denitrification: Effects of limiting nutrients and carbon substrates. *Biotechnology and Bioengineering*, **72**, 25–33.
Chen X T, Zhao B H, Zhang J, Li Y Q, Yang H S, Zhang Y Q. 2023. Rapid start-up of partial nitrification reactor by exogenous AHLs and Vanillin combined with intermittent aeration. *Science of the Total Environment*, **859**, 160191.
Chicano T M, Dietrich L, Almeida N M D, Akram M, Barends T R M. 2021. Structural and functional characterization of the intracellular filament-forming nitrite oxidoreductase multiprotein complex. *Nature Microbiology*, **6**, 1129–1139.
Coelho C, Romao M J. 2015. Structural and mechanistic insights on nitrate reductases. *Protein Science*, **24**, 1901–1911.
Daims H, Lebedeva E V, Pjevac P, Han P, Herbold C, Albertsen M, Jehmlich N, Palatinszky M, Vierheilig J, Bulaev A. 2015. Complete nitrification by *Nitrospira* bacteria. *Nature*, **528**, 504–509.
Denk T R, Mohn J, Decock C, Lewicka-Szczebak D, Harris E, Butterbach-Bahl K, Kiese R, Wolf B. 2017. The nitrogen cycle: A review of isotope effects and isotope modeling approaches. *Soil Biology and Biochemistry*, **105**, 121–137.
Elefsiniotis P, Wareham D G, Smith M O. 2004. Use of volatile fatty acids from an acid-phase digester for denitrification. *Journal of Biotechnology*, **114**, 289–297.
Fang Y T, Koba K, Makabe A, Takahashi C, Zhu W X, Hayashi T, Hokari A A, Urakawa R, Bai E, Houlton B Z, Xi D, Zhang S S, Matsushita K, Tu Y, Liu D W, Zhu F F, Wang Z Y, Zhou G Y, Chen D X, Makita T, *et al.* 2015. Microbial denitrification dominates nitrate losses from forest ecosystems. *Proceedings of the National Academy of Sciences of the United States of America*, **112**, 1470–1474.
Frey C, Hietanen S, Jurgens K, Labrenz M, Voss M. 2014. N and O isotope fractionation in nitrate during chemolithoautotrophic denitrification by *Sulfurimonas gotlandica*. *Environmental Science & Technology*, **48**, 13229–13237.
Füssel J, Lam P, Lavik G, Jensen M M, Holtappels M, Günter M, Kuypers M M M. 2012. Nitrite oxidation in the Namibian oxygen minimum zone. *ISME Journal*, **6**, 1200–1209.
Gao S H, Fan L, Peng L, Guo J H, Agulló-Barceló M, Yuan Z G, Bond P L. 2016. Determining multiple responses of *Pseudomonas aeruginosa* PAO1 to an antimicrobial agent, free nitrous acid. *Environmental Science & Technology*, **50**, 5305–5312.
Ge S J, Peng Y Z, Wang S Y, Lu C C, Cao X, Zhu Y P. 2012. Nitrite accumulation under constant temperature in anoxic denitrification process: The effects of carbon sources and COD/NO_3-N. *Bioresource Technology*, **114**, 137–143.
González P J, Correia C, Moura I, Brondino C D, Moura J J G. 2006. Bacterial nitrate reductases: Molecular and biological aspects of nitrate reduction. *Journal of Inorganic Biochemistry*, **100**, 1015–1023.
Van de Graaf A A, Mulder A, De Bruijn P, Jetten M, Robertson L A, Kuenen J G. 1995. Anaerobic oxidation of ammonium is a biologically mediated process. *Applied and Environmental Microbiology*, **61**, 1246–1251.
Granger J, Sigman D M. 2009. Removal of nitrite with sulfamic acid for nitrate N and O isotope analysis with the denitrifier method. *Rapid Communications in Mass Spectrometry*, **23**, 3753–3762.
Granger J, Sigman D M, Lehmann M F, Tortell P D. 2008. Nitrogen and oxygen isotope fractionation during dissimilatory nitrate reduction by denitrifying bacteria. *Limnology and Oceanography*, **53**, 2533–2545.
Granger J, Sigman D M, Rohde M M, Maldonado M T, Tortell P D. 2010. N and O isotope effects during nitrate assimilation by unicellular prokaryotic and eukaryotic plankton cultures. *Geochimica et Cosmochimica Acta*, **74**, 1030–1040.
Granger J, Wankel S D. 2016. Isotopic overprinting of nitrification on denitrification as a ubiquitous and unifying feature of environmental nitrogen cycling. *Proceedings of the National Academy of Sciences of the United States of America*, **113**, E6391–E6400.
Gregory G, Boyd E F. 2021. Stressed out: Bacterial response to high salinity using compatible solute biosynthesis and uptake systems, lessons from *Vibrionaceae*. *Computational and Structural Biotechnology Journal*, **19**, 1014–1027.
Gruber N, Galloway J N. 2008. An Earth-system perspective of the global nitrogen cycle. *Nature*, **451**, 293–296.
Harms N C, Lahajnar N, Gaye B, Rixen T, Dähnke K, Ankele M, Schwarz-Schampera U, Emeis K C. 2019. Nutrient distribution and nitrogen and oxygen isotopic composition of nitrate in water masses of the subtropical southern Indian Ocean. *Biogeosciences*, **16**, 2715–2732.
Hu X J, Gu H D, Liu J J, Wei D, Zhu P, Cui X A, Zhou B K, Chen X L, Jin J, Liu X B, Wang G H. 2022. Metagenomics reveals divergent functional profiles of soil carbon and nitrogen cycling under long-term addition of chemical and organic fertilizers in the black soil region. *Geoderma*, **418**, 115846.
Jetten M S, Niftrik Lv, Strous M, Kartal B, Keltjens J T, Op den Camp H J. 2009. Biochemistry and molecular biology of anammox bacteria. *Critical Reviews in Biochemistry and Molecular Biology*, **44**, 65–84.
Jiang L, Tang Y X, Sun W H, Yi N, Zhang Y M, Shi H C, Rittmann B E. 2017. Simultaneous di-oxygenation and denitrification in an internal circulation baffled bioreactor. *Biodegradation*, **28**, 195–203.
Karsh K L, Granger J, Kritee K, Sigman D M. 2012. Eukaryotic assimilatory nitrate reductase fractionates N and O isotopes with a ratio near unity. *Environmental Science & Technology*, **46**, 5727–5735.
Kemeny P C, Weigand M, Zhang R, Carter B, Karsh K, Fawcett S, Sigman D M. 2016. Enzyme-level interconversion of nitrate and nitrite in the fall mixed layer of the Antarctic Ocean. *Global Biogeochemical Cycles*, **30**, 1069–1085.
Kobayashi K, Makabe A, Yano M, Oshiki M, Kindaichi T, Casciotti K L, Okabe S. 2019. Dual nitrogen and oxygen isotope fractionation during anaerobic ammonium oxidation by anammox bacteria. *ISME Journal*, **13**, 2426–2436.
Kraft B, Strous M, Tegetmeyer H E. 2011. Microbial nitrate respiration — Genes, enzymes and environmental distribution. *Journal of Biotechnology*, **155**, 104–117.
Kritee K, Sigman D M, Granger J, Ward B B, Jayakumar A, Deutsch C. 2012. Reduced isotope fractionation by denitrification under conditions relevant to the ocean. *Geochimica et Cosmochimica Acta*, **92**, 243–259.
Lam P, Kuypers M M. 2011. Microbial nitrogen cycling processes in oxygen minimum zones. *Annual Review of Marine Science*, **3**,

317–345.
Lehman M F, Sigman D M, Berelson W M. 2004. Coupling the $^{15}N/^{14}N$ and $^{18}O/^{16}O$ of nitrate as a constraint on benthic nitrogen cycling. *Marine Chemistry*, **88**, 1–20.
Leng X Y, Xue D M, Wang Y D, Wang Z L. 2023. Spatial difference of organic composition in farmland soil profile between sea immersion area and non-sea immersion area in Tianjin. *Journal of Tianjin Normal Unierisity* (Natural Science Edition), **43**, 30–37. (in Chinese)
Lipschultz F, Wofsy S C, Ward B B, Codispoti L A, Friedrich G, Elkins J W. 1990. Bacterial transformations of inorganic nitrogen in the oxygen-deficient waters of the Eastern Tropical South Pacific Ocean. *Deep Sea Research* (Part A: Oceanographic Research Papers), **37**, 1513–1541.
Liu W, Huo R, Xu J X, Liang S X, Li J J, Zhao T K, Wang S T. 2017. Effects of biochar on nitrogen transformation and heavy metals in sludge composting. *Bioresource Technology*, **235**, 43–49.
Lu Y C, Li D X, Li C Q, Sun M Y, Wu Z J, Sun Z M. 2022. The effects of 3, 5-dimethylpyrazole on soil nitrification and related enzyme activities in brown soil. *Agronomy Journal*, **12**, 1425.
Lycus P, Einsle O, Zhang L. 2023. Structural biology of proteins involved in nitrogen cycling. *Current Opinion in Chemical Biology*, **74**, 102278.
Mekala L P, Mohammed M, Chinthalapati S, Chinthalapat V. R. 2019. Pyomelanin production: Insights into the incomplete aerobic l-phenylalanine catabolism of a photosynthetic bacterium, *Rubrivivax benzoatilyticus* JA2. *International Journal of Biological Macromolecules*, **126**, 755–764.
Moran M A, Kujawinski E B, Schroer W F, Amin S A, Bates N R, Bertrand E M, Braakman R, Brown C T, Covert M W, Doney S C, Dyhrman S T, Edison A S, Eren A M, Levine N M, Li L, Ross A C, Saito M A, Santoro A E, Segrè D, Shade A, *et al.* 2022. Microbial metabolites in the marine carbon cycle. *Nature Microbiology*, **7**, 508–523.
Pandey C B, Kumar U, Kaviraj M, Minick K J, Mishra A K, Singh J S. 2020. DNRA: A short-circuit in biological N-cycling to conserve nitrogen in terrestrial ecosystems. *Science of the Total Environment*, **738**, 139710.
Pang Y M, Wang J L. 2021. Various electron donors for biological nitrate removal: A review. *Science of the Total Environment*, **794**, 148699.
Paredes I, Otero N, Soler A, Green A J, Soto D X. 2020. Agricultural and urban delivered nitrate pollution input to Mediterranean temporary freshwaters. *Agriculture*, *Ecosystems & Environment*, **294**, 106859.
Pinchbeck B J, Soriano-Laguna M J, Sullivan M J, Luque-Almagro V M, Rowley G, Ferguson S J, Roldan M D, Richardson D J, Gates A J. 2019. A dual functional redox enzyme maturation protein for respiratory and assimilatory nitrate reductases in bacteria. *Molecular Microbiology*, **111**, 1592–1603.
Qi S S, Lin J B, Wang Y L, Yuan S J, Wang W, Xiao L W, Zhan X M, Hu Z H. 2021. Fermentation liquid production of food wastes as carbon source for denitrification: Laboratory and full-scale investigation. *Chemosphere*, **270**, 129460.
Rho E, Evans W. 1975. The aerobic metabolism of cyclohexanecarboxylic acid by *Acinetobacter anitratum*. *Biochemical Journal*, **148**, 11–15.
Richardson D J, Berks B C, Russell D A, Spiro S, Taylor C J. 2001. Functional, biochemical and genetic diversity of prokaryotic nitrate reductases. *Cellular and Molecular Life Sciences*, **58**, 165–178.
Ruan X Y, Yin J, Cui X Y, Li N, Shen D S. 2020. Bioaugmentation and quorum sensing disruption as solutions to increase nitrate removal in sequencing batch reactors treating nitrate-rich wastewater. *Journal of Environmental Sciences*, **98**, 179–185.
Schneider S, Mohamed M E S, Fuchs G. 1997. Anaerobic metabolism of L-phenylalanine via benzoyl-CoA in the denitrifying bacterium *Thauera aromatica*. *Archives of Microbiology*, **168**, 310–320.
Sigman D M, Casciotti K L, Andreani M, Barford C, Galanter M, Böhlke J. 2001. A bacterial method for the nitrogen isotopic analysis of nitrate in seawater and freshwater. *Analytical Chemistry*, **73**, 4145–4153.
Sigman D M, Granger J, Difiore P J, Lehmann M M, Ho R, Cane G, Geen A V. 2006. Coupled nitrogen and oxygen isotope measurements of nitrate along the eastern North Pacific margin. *Global Biogeochemical Cycles*, **20**, GB100.
Singh S, Anil A G, Kumar V, Kapoor D, Subramanian S, Singh J, Ramamurthy P C. 2022. Nitrates in the environment: A critical review of their distribution, sensing techniques, ecological effects and remediation. *Chemosphere*, **287**, 131996.
Sparacino-Watkins C, Stolz J F, Basu P. 2014. Nitrate and periplasmic nitrate reductases. *Chemical Society Reviews*, **43**, 676–706.
Strous M, Kuenen J G, Jetten M S. 1999. Key physiology of anaerobic ammonium oxidation. *Applied and Environmental Microbiology*, **65**, 3248–3250.
Su X X, Wang Y Y, He Q, Hu X B, Chen Y. 2019. Biochar remediates denitrification process and N_2O emission in pesticide chlorothalonil-polluted soil: role of electron transport chain. *Chemical Engineering Journal*, **370**, 587–594.
Sun X, Ji Q X, Jayakumar A, Ward B B. 2017. Dependence of nitrite oxidation on nitrite and oxygen in low oxygen seawater. *Geophysical Research Letters*, **44**, 7883–7891.
Tan Q Y, Zhang G Y, Ding A Z, Bian Z Y, Wang X, Xing Y Z, Zheng L. 2023. Anthropogenic land-use activities within watersheds reduce comammox activity and diversity in rivers. *Journal of Environmental Management*, **338**, 117841.
Tomei M C, Annesini M C. 2005. 4-Nitrophenol biodegradation in a sequencing batch reactor operating with aerobic-anoxic cycles. *Environmental Science & Technology*, **39**, 5059–5065.
Treibergs L A, Granger J. 2017. Enzyme level N and O isotope effects of assimilatory and dissimilatory nitrate reduction. *Limnology and Oceanography*, **62**, 272–288.
Vadivelu V M, Yuan Z, Fux C, Keller J. 2006. The inhibitory effects of free nitrous acid on the energy generation and growth processes of an enriched *Nitrobacter* culture. *Environmental Science & Technology*, **40**, 4442–4448.
Valiente N, Gil-Márquez J M, Gómez-Alday J J, Andreo B. 2020. Unraveling groundwater functioning and nitrate attenuation in evaporitic karst systems from southern Spain: An isotopic approach. *Applied Geochemistry*, **123**, 104820.
Wang A, Fang Y T, Chen D X, Phillips O, Koba K, Zhu W X, Zhu J J. 2018. High nitrogen isotope fractionation of nitrate during denitrification in four forest soils and its implications for denitrification rate estimates. *Science of the Total Environment*, **633**, 1078–1088.
Wang H, Zhang J Q, Zhang Y F, Li J F, Li F L, Strydonck M V, Hendrix V. 2000. Chronology of the Chenier I and shoreline changes since the last 1ka, on western coast of Bohai Bay. *Marine Geology* & *Quat Ernary Geology*, **20**, 7–14. (in Chinese)
Wang L, Li Y M, Ma N, Gu G W. 2009. Effects of pyridine and methanol on the biodegradation of 2-methylpyridine by activated sludge under denitrifying conditions. In: *International Conference on Energy and Environment Technology*. IEEE, Guilin, China. pp. 618–621.
Wang Q, Garrity G M, Tiedje J M, Cole J R. 2007. Naive Bayesian classifier for rapid assignment of rRNA sequences into the new bacterial taxonomy. *Applied and Environmental Microbiology*, **73**, 5261–5267.
Wang S Y, Radny D, Huang S B, Zhuang L J, Zhao S Y, Berg M, Jetten M S, Zhu G B. 2017. Nitrogen loss by anaerobic ammonium oxidation in unconfined aquifer soils. *Scientific Reports*, **7**, 40173.
Wang Z F, Zhang Y J, Li X, Li J K, Zhao Z M, Hou X. 2023. Mixed culture of plants improved nutrient removal in constructed wetlands: Response of microbes and root exudates. *Environmental Science and Pollution Research*, **30**, 5861–5872.
Wei Q, Zhang J S, Luo F Z, Shi D H, Liu Y C, Liu S, Zhang Q, Sun W Z, Yuan J L, Fan H T. 2022. Molecular mechanisms through which different carbon sources affect denitrification by *Thauera linaloolentis*: Electron generation, transfer, and competition. *Environment International*, **170**, 107598.
Welte C U, Rasigraf O, Vaksmaa A, Versantvoort W, Arshad A, Op den Camp H J, Jetten M S, Lüke C, Reimann J. 2016. Nitrate- and nitrite-dependent anaerobic oxidation of methane. *Environmental Microbiology Reports*, **8**, 941–955.
Wenk C B, Zopfi J, Blees J, Veronesi M, Niemann H, Lehmann M F. 2014. Community N and O isotope fractionation by sulfide-dependent denitrification and anammox in a stratified lacustrine water column. *Geochimica et Cosmochimica Acta*, **125**, 551–563.
Wunderlich A, Meckenstock R, Einsiedl F. 2012. Effect of different carbon substrates on nitrate stable isotope fractionation during microbial denitrification. *Environmental Science & Technology*, **46**, 4861–4868.
Wunderlich A, Meckenstock R U, Einsiedl F. 2013. A mixture of nitrite-oxidizing and denitrifying microorganisms affects the $\delta^{18}O$ of dissolved nitrate during anaerobic microbial denitrification depending on the $\delta^{18}O$ of ambient water. *Geochimica et*

Cosmochimica Acta, **119**, 31–45.
Xue D M, Baets B D, Vermeulen J, Botte J, Cleemput O V, Boeckx P. 2010. Error assessment of nitrogen and oxygen isotope ratios of nitrate as determined via the bacterial denitrification method. *Rapid Communications in Mass Spectrometry*, **24**, 1979–1984.
Xue D M, Botte J, Baets B D, Accoe F, Nestler A, Taylor P, Cleemput O V, Berglund M, Boeckx P. 2009. Present limitations and future prospects of stable isotope methods for nitrate source identification in surface- and groundwater. *Water Research*, **43**, 1159–1170.
Xue D M, Yu H, Fang Y T, Shan J, Xi D, Wang Y D, Kuzyakov Y, Wang Z L. 2020. ^{15}N-tracer approach to assess nitrogen cycling processes: Nitrate reduction, anammox and denitrification in different pH cropland soils. *Catena*, **193**, 104611.
Yue F J, Liu X L, Li J, Zhu Z Z, Wang Z L. 2010. Using nitrogen isotopic approach to identify nitrate sources in waters of Tianjin, China. *Bulletin of Environmental Contamination and Toxicology*, **85**, 562–567.
Zhan M J, Zeng W, Wu C C, Chen G X, Meng Q A, Hao X J, Peng Y Z. 2024. Impact of organic carbon on sulfide-driven autotrophic denitrification: Insights from isotope fractionation and functional genes. *Water Research*, **255**, 121507.
Zhang D D, Li M Y, Yang Y C, Yu H, Xiao F S, Mao C Z, Huang J, Yu Y H, Wang Y F, Wu B, Wang C, Shu L F, He Z L, Yan Q Y. 2022. Nitrite and nitrate reduction drive sediment microbial nitrogen cycling in a eutrophic lake. *Water Research*, **220**, 118637.
Zhao J F, Yang J Q, Xie H F, Qin X, Huang R X. 2024. Sustainable management strategies for balancing crop yield, water use efficiency and greenhouse gas emissions. *Agricultural Systems*, **217**, 103944.
Zheng W B, Wang S Q, Tan K D, Lei Y P. 2020. Nitrate accumulation and leaching potential is controlled by land-use and extreme precipitation in a headwater catchment in the North China Plain. *Science of the Total Environment*, **707**, 136168.
Zhou Y, Oehmen A, Lim M, Vadivelu V, Ng W J. 2011. The role of nitrite and free nitrous acid (FNA) in wastewater treatment plants. *Water Research*, **45**, 4672–4682.
Zhu Q, Liang Y F, Zhang Q, Zhang Z Y, Wang C P, Zhai S, Li Y H, Sun H W. 2023. Biochar derived from hydrolysis of sewage sludge influences soil properties and heavy metals distributed in the soil. *Journal of Hazardous Materials*, **442**, 130053.
Zhu Y S, Wang Y D, Guo C C, Xue D M, Li J, Chen Q, Song Z L, Lou Y L, Kuzyakov Y, Wang Z L. 2020. Conversion of coastal mars4hes to croplands decreases organic carbon but increases inorganic carbon in saline soils. *Land Degradation & Development*, **31**, 1099–1109.

Executive Editor-in-Chief Jinshui Wu
Managing Editor Lujuan Sun